JOURNAL OF CHEMICAL INFORMATION AND MODELING

Article

pubs.acs.org/jcim

Identification of Possible Binding Sites for Morphine and Nicardipine on the Multidrug Transporter P-Glycoprotein Using Umbrella Sampling Techniques

Nandhitha Subramanian,[†] Karmen Condic-Jurkic,[†] Alan E. Mark,[†,§] and Megan L. O'Mara*[,†,‡,⊥]

[†]School of Chemistry and Molecular Biosciences, [§]The Institute for Molecular Biosciences, and [‡]School of Mathematics and Physics, University of Queensland, Brisbane, QLD 4072, Australia

Supporting Information

ABSTRACT: The multidrug transporter P-glycoprotein (P-gp) is central to the development of multidrug resistance in cancer. While residues essential for transport and binding have been identified, the location, composition, and specificity of potential drug binding sites are uncertain. Here molecular dynamics simulations are used to calculate the free energy profile for the binding of morphine and nicardipine to P-gp. We show that morphine and nicardipine primarily interact with key residues implicated in binding and transport from mutational studies, binding at different but overlapping sites within the transmembrane pore. Their permeation pathways were distinct but involved overlapping sets of residues. The results indicate that the binding location and permeation pathways of morphine and nicardipine are not well separated and cannot be considered as unique. This has important implications for our understanding of substrate uptake and transport by P-gp. Our results are independent of the choice of starting structure and consistent with a range of experimental studies.

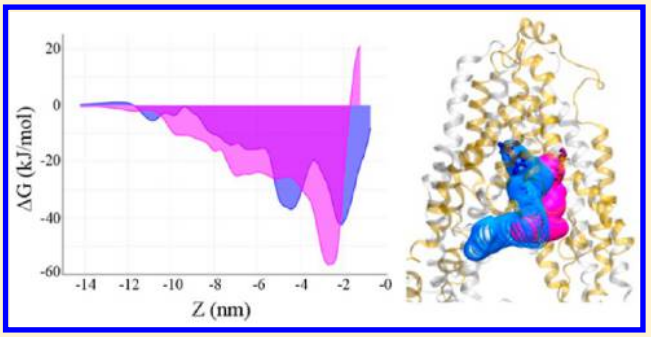

INTRODUCTION

Multidrug resistance presents a major obstacle to the successful treatment of diseases ranging from bacterial infections to cancer. In many cases, multidrug resistance results from the overexpression of membrane-embedded efflux proteins. One such efflux protein is P-glycoprotein (P-gp), the major human multidrug transporter. The expression of P-gp in cancer cells confers resistance to chemotherapeutic agents. P-gp transports over 120 different pharmaceuticals, steroids, and peptides and plays a key role in the uptake and excretion of a wide range of therapeutic drugs.[1] Despite extensive research over 38 years, neither the physical location of any binding site nor the nature of the interaction between P-gp and its transport substrates has been fully characterized.

P-gp is a transmembrane (TM) protein that belongs to the ATP-binding cassette (ABC) transporter family of proteins. All ABC transporters, including P-gp, use the energy of ATP hydrolysis to transport a wide range of molecules out of the cell. As shown in Figure 1, P-gp is composed of two transmembrane domains (TMDs), each made up of six TM helices that associate to form a TM pore, and two cytosolic nucleotide-binding domains (NBDs). The TMDs are involved in substrate recognition and efflux, while the binding and hydrolysis of ATP at the NBDs are coupled to the transport of substrate across the TMDs. It has long been proposed that substrate transport is associated with the TMDs adopting an inward- or an outward-facing conformation, in which the TM pore is open to the cytosolic side or the extracellular side of the membrane, respectively.[2] The structures of several homologous ABC transporters[3−11] obtained under different crystallization conditions, such as the presence or absence of nucleotides, display a range of inward-facing and outward-facing conformations. It has been postulated that these crystallographic conformations represent a spectrum of distinct states in the proposed transport cycle. Further experimental studies have demonstrated that the addition of a transport substrate to purified P-gp reconstituted in lipid vesicles increases the ATPase activity of P-gp,[12] suggesting that the binding of substrate may drive the hydrolysis of ATP.

Various studies have attempted to elucidate the physical location of a substrate binding site within the TM pore. In particular, these studies have sought to identify key residues or interactions that would enable P-gp to discriminate between different classes of compounds. To date, no crystal structure of P-gp with a bound transport substrate has been solved. Instead, P-gp has only been crystallized in complex with cyclic peptide inhibitors[4,11] and nanobodies.[10] Given that no crystal structure of P-gp with bound substrate is available, the majority of the information related to possible binding sites has been inferred from mutational studies, which have been used to identify residues that affect the transport rate and binding affinity of different substrates.[13−15] While the residues identified are distributed throughout P-gp, including within the NBDs, the

Received: December 15, 2014
Published: May 4, 2015

DOI: 10.1021/ci5007382
J. Chem. Inf. Model. 2015, 55, 1202−1217

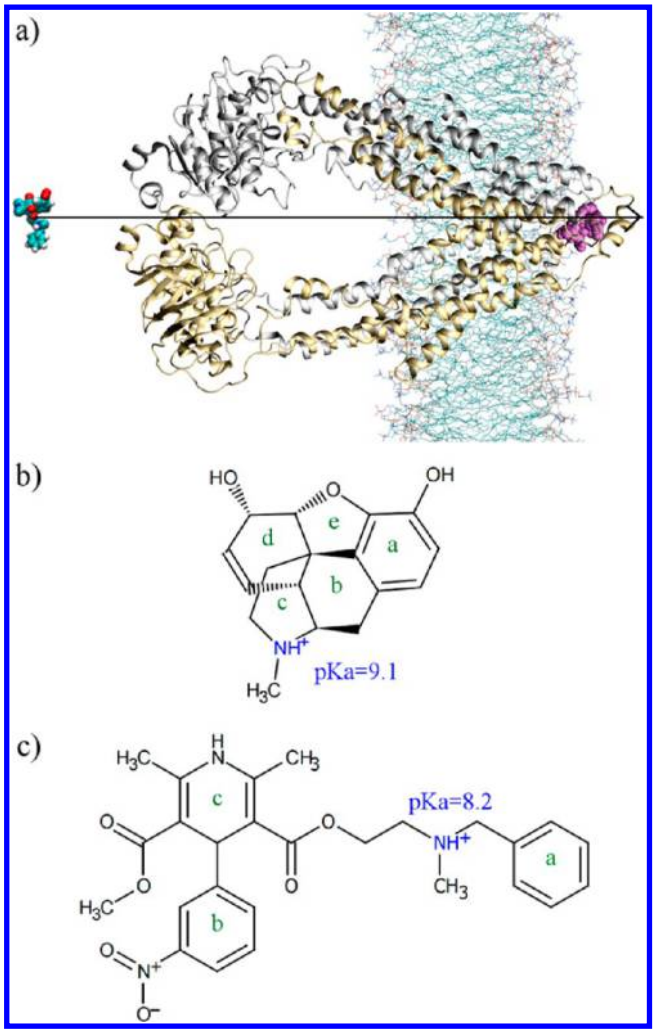

Figure 1. Equilibrated membrane-embedded P-glycoprotein (P-gp). (a) The initial configuration of membrane-embedded P-gp used in the umbrella sampling simulations. The black line represents the reaction coordinate (*Z*-axis) along which the substrate is moved. The N-terminal and C-terminal halves are shown in gold and silver cartoon representation, respectively. The membrane is shown in line representation. The substrate morphine or nicardipine (CPK spacefill) was placed at a distance of 15 nm from the reference group of P-gp (purple spacefill). The structures of (b) morphine and (c) nicardipine at pH 7.0. The pK_a values of ionizable groups are shown in blue. The rings of morphine (a−e) and nicardipine (a−c) are labeled in green.

majority of the residues known to affect transport rates are clustered in the TM region. In addition, FRET experiments involving Hoechst 33342 suggested that the physical location of the primary binding site for substrates lies in the membrane-embedded region of TMDs, within the span of the intracellular leaflet.[16] In particular, the binding of different substrates has been proposed to be associated with residues within TM helices 4, 5, 6, 10, 11, and 12.[17] However, residues from other TM helices have also been shown to affect the ability of P-gp to transport substrates, and thus, it has not been possible to identify the physical location of a single specific substrate binding site.[14,15] Some experimental results have been interpreted as suggesting that P-gp contains multiple sites, which interact with different classes of substrate. For example, photoaffinity labeling studies have shown that verapamil binds competitively to vincristine, whereas azidopine and vinblastine bind noncompetitively.[18,19] Using equilibrium binding studies and competition/modulation studies examining the effect of combinations of substrates on ATP hydrolysis, Martin et al. suggested that there might be four pharmacologically distinct interaction sites in P-gp.[20] Others have proposed that P-gp has as many as seven distinct substrate interaction sites.[13] Despite this, the molecular composition of any of the proposed sites has not been elucidated in detail. As certain residues appear to interact with multiple classes of substrate, it has also been suggested that the TMDs collectively form a single nonspecific binding pocket.[14,21]

For example, Figure 2 shows the residues within the TM region of P-gp that affect the binding and/or transport of four

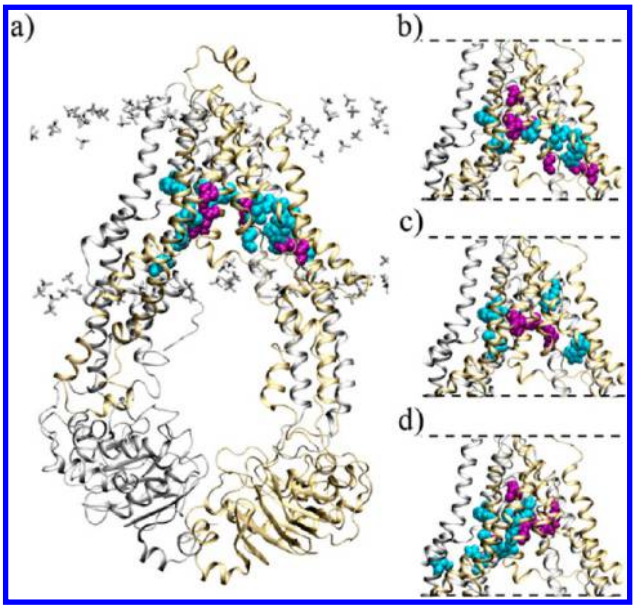

Figure 2. Spatial distribution of experimentally identified residues involved in the binding and/or transport of P-gp substrates. (a) The equilibrated membrane-embedded P-gp system with residues affecting the binding (cyan) or transport (purple) of verapamil shown in spacefill representation. The N-terminal (gold) and C-terminal (silver) halves of P-gp are shown in cartoon representation. Phosphate groups associated with the lipid heads are shown in licorice representation. A truncated view of the membrane-embedded region of P-gp showing the residues experimentally implicated in (b) vinblastine, (c) colchicine, and (d) Rhodamine binding (cyan) and transport (purple). The dotted lines in (b), (c), and (d) give the span of the lipid membrane.

commonly studied P-gp transport substrates: verapamil,[17,22−29] vinblastine,[17,23−27,29,30] colchicine,[17,23,24,26−28] and Rhodamine 123.[28−32] Figure 2a shows the equilibrated structure of membrane-embedded P-gp, highlighting the residues within the TMDs that are primarily implicated in the binding (cyan) and transport (purple) of verapamil. In contrast, Figure 2b−d shows the corresponding residues within the TMDs associated with the binding and/or transport of vinblastine, colchicine, and Rhodamine 123, respectively. These residues are listed in Table 1. On the basis of competitive binding studies, it has been proposed that verapamil and vinblastine interact with the same site in P-gp, commonly referred to as the vinblastine site.[13,33] In a similar manner, colchicine and Hoechst 33342 have also been proposed to bind to P-gp at a separate pharmacological site, the H-site or Hoechst site.[34,35] Rhodamine 123 and related molecules have been proposed to bind

DOI: 10.1021/ci5007382
J. Chem. Inf. Model. 2015, 55, 1202−1217

Table 1. Residues within the Transmembrane Region of Membrane-Embedded P-gp That Affect the Experimental Binding and Transport of P-gp Substrates

P-gp substrates	binding residues	ref	transport residues	ref
verapamil[a]	L335	22	S218	17
	V978	23	L335, A338, I864, G980	22
	G935, F938, T941, Q942, A943	24	A981	23
	I302	25	Q128	29
	F724	26		
	H60, G63, L64	27		
	A298, L335, G868, F938, Q942	28		
	V978, S989	28		
vinblastine[b]	A943	24	S218, G868	17
	I302	25	L335, L971, V978	23
	F724	26	T941, Y946, Y949	24
	H60, G63	27	Q128	29
	L64, T195, I302	30		
colchicine[c]	Q942	24	S218	17
	F724	26	L335, L971, V978	23
	H60, L64	27		
	F766, M982, A983	28		
Rhodamine[d]	F724	26	Q769	29
	F332, F766, F979, M982, A983	28	L335	30
	Q986	28	L64, I336, A837, L971, V978	31
	F339	30		
	Y949	32		

[a]Figure 2a. [b]Figure 2b. [c]Figure 2c. [d]Figure 2d.

to a third pharmacologically distinct site, the R-site or Rhodamine site.[35] While vinblastine, Hoechst 33342, and Rhodamine 123 bind noncompetitively with one another, it is evident from Figure 2 that in each of these cases, the residues involved in binding and transport are not spatially well separated.

Further examination of all the residues implicated in binding and transport indicates that a key subset of residues is involved in the binding or transport of multiple substrates, irrespective of whether they are competitive or noncompetitive substrates. For example, Table 1 shows that His60, Leu64, Phe724, and Gln942 are all implicated in the binding of the noncompetitive substrate pair colchicine and verapamil,[23,26,27] while two of these residues, Leu64 and Phe724, together with Tyr949, are implicated in the binding or transport of a second noncompetitive substrate pair, Rhodamine and vinblastine.[24,26,30] In addition, Leu335 and Val978 are implicated in binding of verapamil, but not colchicine, Rhodamine or vinblastine; and are implicated in the transport of all four substrates (Table 1). While conformational changes during substrate transport cannot be excluded, the close spatial proximity of these residues suggests that the binding locations are not truly independent or distinct.

In recent years, a number of computational approaches have been used in an attempt to characterize potential substrate binding sites in P-gp. These include molecular docking and pharamacophore mapping studies.[36−40] In two independent studies, Ferreira et al.[36] and Tarcsay and Keserű[37] examined the interaction of various P-gp substrates such as Rhodamine 123, vinblastine, verapamil and Hoechst 33342 with P-gp using molecular docking studies. In one of these studies, 45 residues were implicated in the binding of Hoechst 33342.[36] In the other, only 28 residues were proposed to form the Hoechst site.[37] Critically, only three residues, Gln191, Gln343, and Ser340, were common to both studies.[36,37] Likewise the Rhodamine 123 binding sites proposed by these two docking studies only contain four common residues out of 49[36] and 31[37] residues, respectively. On the basis of pharmacophore mapping, Silva et al.[38] also proposed a set of residues corresponding to the colchicine binding site. In this case there is no overlap at all with those proposed by Tarcsay and Keserű.[37] In contrast to these studies, both Klepsch et al.[39] and Chufan et al.[40] used independent docking and binding studies to conclude that the inhibitors propafenone, tariquidar, cyclosporine A and valinomycin could bind at multiple locations within the TM region, and thus it was not possible to identify unique binding sites for these molecules.

Molecular dynamics (MD) simulation is another computational approach that has been used extensively to provide insight into the nature of substrate recognition and binding by P-gp and its homologues. For example, Jara et al.[41] docked two inhibitors, a propafenone derivative (GP-240) and tariquidar (XR9576), into the P-gp TMD region and used these complexes to initiate a series of MD simulations. Their results were consistent with the findings of Klepsch et al.[39] and Chufan et al.:[40] both inhibitors interacted with residues from multiple TM helices with considerable overlap. Here, TM helices 4, 5, 6, 7, 8, 9, and 12 were implicated in the binding of tariquidar, while TM helices 4, 5, 6, 7, and 12 were implicated in the binding of GP-240. It is important to note that, during these simulations, the protein was held fixed and only minor changes in the side chain orientations were observed compared to the initial docked conformations. In another study using an homology model of human P-gp, Zhang et al.[42] placed paclitaxel or doxorubicin at the intracellular entrance to the TM pore and performed a series of free MD simulations to determine whether either drug entered the TM pore. They found that both substrates spontaneously moved into the TM pore, close to the central plane of the membrane. On the basis of their observations, Zhang et al.[42] proposed that in human P-gp, Phe303 played a major role in the interaction with paclitaxel; however, they did not identify distinct binding sites.

Other studies have attempted to understand how the binding of substrates affects the overall conformation of P-gp. For example, Ma and Biggin[43] suggested that the binding of daunorubicin within the TM region perturbed the dimerization of the NBDs. Simulations have also been used to shed light on how substrates or inhibitors may enter the TM region from the membrane or solvent. Using a combination of MD simulations and data from double electron−electron resonance (DEER) spectroscopy, Wen et al.[44] analyzed the extent to which a membrane-embedded P-gp could adopt a range of conformations. During one of these simulations, Wen et al. observed a partial protrusion of a lipid tail into the TM pore through the cleft formed by the membrane-embedded regions of TM helices 4 and 6.[44] They claim that the protrusion of this lipid tail into P-gp supports the proposed role of this cleft as a possible lipid-accessible substrate uptake portal.[4−11]

Despite all of these previous experimental and theoretical studies, the basic question of whether there are distinct binding

DOI: 10.1021/ci5007382
J. Chem. Inf. Model. 2015, 55, 1202−1217

sites for different classes of substrates, or one single overlapping binding region, has remained a matter of continuing debate. Given the difficulties in working with purified and reconstituted P-gp, simulation based approaches would appear to hold the most promise in shedding light on these issues. Simulations have played a role in resolving the dynamic structural mechanism by which ABC transporters, such as P-gp, function. For example, the MD studies carried out using isolated ABC transporter NBDs[45−49] have provided information on the conformational changes that occur on ATP binding and after the hydrolysis of ATP to ADP. MD simulations of P-gp and other full-length ABC transporters have also been used to examine conformational changes within the TMDs and their possible role in transporter function.[41−44,50−58] In addition, simulations of mouse P-gp[51,52] have highlighted the importance of the lipid composition of the membrane environment, Mg^{2+} and the protonation state of specific residues in determining the physiologically relevant state of the protein.

In this study, we have used a combination of MD simulations and umbrella sampling techniques to investigate the interactions between membrane-embedded mouse P-gp and two substrates, morphine and nicardipine. Specifically, umbrella sampling techniques have been used to calculate the potential of mean force (PMF) associated with the binding of these two P-gp substrates along an axis normal to the plane of the membrane projecting through the center of P-gp. The aim was to identify the specific locations within the translocation pore where the substrates form stable interactions with P-gp. MD simulations have also been used to examine whether the two substrates would bind spontaneously to the locations identified from the corresponding PMFs on a 100 ns time scale. Previous docking and simulation studies of the interaction of substrates or inhibitors with P-gp have primarily relied on homology models, which by their very nature are uncertain,[36,37,41,59] or on crystal structures of the protein outside of a membrane environment,[43,44,57,58] the physiological relevance of which has been questioned. In contrast, the current work is based on an extensively equilibrated structure of membrane-embedded apo mouse P-gp that has been demonstrated to reproduce a wide range of experimental cross-linking studies.[51] In fact, this structure predicted changes in the TM helices that were later confirmed in revisions to the published crystal structures.[10,11]

The substrates morphine and nicardipine were chosen for this work based on a combination of biochemical and computational criteria. Most P-gp substrates contain aromatic or cyclic groups and are primarily hydrophobic in nature. As such, they bind to and interact with lipid bilayers. However, almost all substrates also contain at least one positively charged group, most commonly a tertiary amine that is protonated at neutral pH, and thus have an overall charge of +1 at physiological pH. P-gp substrates range in size from large complex molecules such as vinblastine (811 amu), to smaller molecules such as morphine (285 amu). In this study, we compare morphine, a small and compact substrate, with nicardipine (479 amu) a medium-sized, elongated substrate. As shown in Figure 1, both are predominantly hydrophobic, but carry a charge of +1 at neutral pH. Morphine is a potent natural opiate and the most common analgesic used for the treatment of pain associated with cancer. It also plays an important part in the regulation of neoplastic tissue.[60,61] Morphine is one of the smallest P-gp substrates[62] and has a rigid pentacyclic structure, making it computationally efficient to simulate. Drug accumulation studies by Callaghan et al. examined the binding of radiolabeled morphine, vinblastine, and verapamil to the membranes of cell lines overexpressing or not expressing P-gp. They found that vinblastine and verapamil could displace membrane-bound morphine in cell lines expressing P-gp.[62] These results suggest that morphine competes for binding and transport with verapamil and vinblastine. In contrast, the calcium channel blocker nicardipine is believed to bind to P-gp in a noncompetitive manner to morphine. Nicardipine enhances the effects of antineoplastic agents, leading to chemo-sensitivity in tumor cells, and has been extensively used experimentally in drug binding/transport studies of P-gp.[63,64] Studies by Martin et al. and Pascaud et al. suggested that nicardipine binds to a site different to that of both vinblastine and Hoechst.[20,33]

In the next section, the methodology used in the simulations and analysis is described in detail. The steps taken to ensure the convergence of the PMFs are also presented. The implications of the PMFs obtained are discussed in terms of the residues with which the two substrates interact, and whether there is a single or multiple binding sites. Finally, a model is presented that can be used to reconcile the fact that classes of substrates bind competitively with each other but noncompetitively with other classes given our current understanding of the binding region of P-gp.

METHODOLOGY

Two sets of MD simulations were performed. In order to identify the binding sites for morphine and nicardipine, the PMF for each of these substrates was calculated along an axis projecting through the center of P-gp normal to the plane of the membrane as described below. To examine whether morphine and nicardipine would bind spontaneously to the sites identified on a nanosecond time scale, a series of free MD simulations were also performed.

Simulation Setup. The starting configuration for all MD simulations performed here was based on an equilibrated conformation of P-gp (PDB ID: 3G5U) embedded in a 10:1 2-oleoyl-1-palmitoyl-*sn*-glycero-3-phosphocholine (POPC) and cholesterol bilayer obtained by O'Mara and Mark.[51] The coordinates of this system were downloaded from the Automated Topology Builder (ATB) and repository.[65] Note that, whereas in the work of O'Mara and Mark the N- and C-termini were artificially neutralized, in this work the N- and C-termini were acetylated and aminated, respectively. All MD simulations were performed using GROMACS[66] version 3.3.3 in conjunction with the GROMOS 54A7 forcefield for proteins.[67] The simple point charge (SPC) water model[68] was used to describe the solvent water. The parameters for POPC were taken from Poger et al.[69] The parameters for cholesterol and simulation conditions were the same as those used by O'Mara and Mark.[51] All simulations were performed under periodic boundary conditions in a rectangular box. The dimensions of the box were chosen such that the minimum distance of the protein to the box wall was at least 1.0 nm. A twin-range method was used to evaluate the nonbonded interactions. Interactions within the short-range cutoff of 0.8 nm were updated every step. Interactions within the long-range cutoff of 1.4 nm were updated every 8 fs, together with the pair list. A reaction field correction was applied using a relative dielectric constant of ε_r = 78.5, to minimize the effect of truncating the electrostatic interactions beyond the 1.4 nm long-range cutoff.[70] A value of ε_r = 78.5 was used, as this is the experimental relative dielectric constant for water at ∼300 K.

DOI: 10.1021/ci5007382
J. Chem. Inf. Model. 2015, 55, 1202−1217

Note that, while a range of other values have been used with SPC water to attempt to match the reaction field to different calculated values for the dielectric constant of SPC water, the properties of water have been shown to be insensitive to small changes in the relative dielectric constant beyond the 1.4 nm cutoff.[71] The LINCS algorithm[72] was used to constrain the lengths of the covalent bonds. The geometry of the water molecules was constrained using the SETTLE algorithm.[73] In order to extend the time scale that could be simulated, explicit hydrogen atoms in the protein were replaced with dummy atoms, the positions of which were calculated at each step on the basis of the positions of the heavy atoms to which they were attached. This eliminates high-frequency degrees of freedom associated with the bond angle vibrations involving hydrogens. These degrees of freedom are largely uncoupled from the rest of the protein and their elimination allows a time step of 4 fs to be used to integrate the equations of motion without affecting thermodynamic properties of the system significantly, as discussed by Feenstra et al.[74] The simulations were carried out in the NPT ensemble at T = 300 K, and P = 1 bar. The temperature and pressure were maintained close to the reference values by weakly coupling the system to an external temperature[75] and pressure bath using a relaxation time constant of 0.1 and 0.5 ps, respectively. The pressure coupling was semi-isotropic. Data was collected for analysis every 25 ps during the PMF calculations and every 50 ps during the unbiased MD simulations. Images were produced using VMD.[76]

P-gp Substrates. The initial coordinates of the P-gp substrates morphine and nicardipine were taken from PubChem Substance and Compound database.[77] The protonation state of morphine and nicardipine at pH 7.0 was determined by calculating the ionization constant of each titratable group in the compound, using the algorithm implemented in ChemAxon.[78,79] At pH 7.0, the tertiary amine of morphine and that of nicardipine were predicted to be protonated, resulting in a +1 charge on each molecule. The pK_a values of the tertiary amine groups, and the cyclic groups of morphine (a−e) and nicardipine (a−c) are shown in Figure 1. Parameters for morphine and nicardipine in the protonated state at pH 7.0 were developed using the ATB and Repository.[65] The ATB generates parameters for small molecules based on the GROMOS 54A7 force field.[67] The parameters produced by the ATB have been demonstrated to perform well in the SAMPL4 blind computational challenge in which the calculated hydration free enthalpies of drug-like molecules are compared to experimental results.[80] The ATB can generate fully refined parameters for molecules that contain less than 50 atoms. As nicardipine contains 86 atoms the interaction parameters were obtained by subdividing nicardipine into a series of overlapping chemical entities each containing less than 50 atoms. These were then submitted separately to the ATB. The final set of parameters used to describe nicardipine was obtained by combining these fragments. The final parameters obtained are available for download from the ATB (MOL IDs: 5089 and 2009).[65] Note that these parameters maintain the conformation of both morphine and nicardipine within <0.1 nm (all-atom root-mean-squared deviation (RMSD)) from the conformation optimized at the B3LYP/6-31G* level of theory in implicit solvent.[65]

Potential of Mean Force Calculations. The PMF of morphine or nicardipine along the central axis of P-gp was calculated using the umbrella sampling method.[81] To initiate the simulations, a group of eight residues (Ala79, Ser80, Val81, Gly82, Asn83, Val84, Ser85, and Lys86) from the extracellular region of TM1 was chosen as a reference group. A single molecule of the substrate was placed at a distance of 15.0 nm on the cytosolic side from the reference group of P-gp, along the chosen reaction coordinate defined as the axis passing through the reference group and normal to the membrane. The initial position of the substrate relative to P-gp, and the direction of the reaction coordinate are shown in Figure 1. A harmonic restraint with a force constant of 500 kJ/(mol·nm^2) was applied to the center of mass (COM) of the substrate and moved along the reaction coordinate toward the reference group at a rate of 15 nm/ns. This simulation was used to generate a set of 15 reference configurations separated by 1.0 nm intervals along the reaction coordinate. These were then used as starting configurations for umbrella sampling calculations at intermediate distances spaced every 0.25 nm along the reaction coordinate giving 60 windows in total. In each umbrella sampling simulation, the COM of the substrate was harmonically restrained using a force constant of 500 kJ/(mol·nm^2) in the Z-direction to allow it to sample a specific region (window) along the reaction coordinate. To reduce the effect of any directional bias induced during the generation of the reference configurations on the final PMF, the starting configuration for each of the intermediate distances were selected randomly from the two adjacent reference configurations. The motion of the substrate was not restrained in the XY plane.

The PMF was obtained by integrating the derivative of the free energy with respect to the distance along the reaction coordinate as described by Kaestner and Thiel.[82,83] The system was simulated at each distance corresponding to a specific umbrella sampling window along the reaction coordinate until the derivative of the free energy had converged. The derivative of free energy was considered to have converged when the difference between the average of the derivative calculated for a series of 1 ns sliding windows taken every 0.5 ns did not vary by more than 5 kJ/mol over a period of 5 ns (10 windows). The time for each window to meet the convergence criteria is given as Supporting Information (Table S1). Once the system was considered to have converged, the simulation was extended for a further 10 ns. The average derivative over these final 10 ns was used in the calculation of the PMF. The standard error in the derivative of the free energy was also calculated over the final 10 ns.

Simulations of Spontaneous Binding. To examine if morphine or nicardipine would bind spontaneously to the binding locations identified on a nanosecond time scale, eight molecules of the substrate were placed randomly in the water layer surrounding P-gp. As both morphine and nicardipine carry a +1 charge, eight Cl^- counterions were added to neutralize the system. The membrane-embedded P-gp system was already equilibrated prior to the addition of eight substrate molecules. Nevertheless, 1000 steps of steepest descent energy minimization was performed to relax the solvent around the substrate. A 50 ps simulation was then performed in which the backbone of the protein was position restrained using a harmonic potential with a force constant of 500 kJ/(mol·nm^2). Starting from this configuration, three independent simulations without restraints were then performed by assigning new velocities in each case. Each simulation was 80 ns in length.

Effect of Starting Structure on Substrate Binding. In order to determine whether the interactions of morphine and

DOI: 10.1021/ci5007382
J. Chem. Inf. Model. 2015, 55, 1202−1217

nicardipine with the TMDs of P-gp observed in the simulations were biased by the choice of the P-gp starting structure, a series of MD simulations based on a revised mouse P-gp structure (PDB ID: 4M1M)[11] were also performed. The 4M1M P-gp structure was extensively equilibrated in a POPC and cholesterol membrane (POPC:cholesterol, 10:1) as described in the methods under similar conditions to those used by O'Mara and Mark used to equilibrate 3G5U.[51] The two substrates, morphine and nicardipine were placed within the TM pore of the equilibrated 4M1M structure at $Z = -2.5$ nm for morphine and $Z = -2.3$ nm for nicardipine, corresponding to their respective free energy minimum shown in Figure 3.

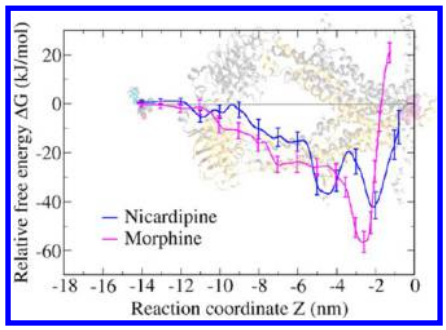

Figure 3. Potential of mean force of morphine (pink) and nicardipine (blue) in P-gp as a function of the reaction coordinate (Z). A plot of the PMFs of morphine and nicardipine are superimposed on the membrane-embedded P-gp structure (cartoon). The distances along the reaction coordinate are calculated with respect to the center of mass of the reference group (purple spacefill). The error bars reflect the accumulated error along the PMF.

Though the 4M1M P-gp structure was equilibrated before the addition of the substrates, 1000 steps of steepest descent energy minimization was performed in each case to relax the solvent around the substrate. In each case, a free MD simulation of 40 ns was performed.

Analysis. *Calculation of the Spatial Density Function.* In order to calculate the spatial distribution of the substrates during the MD simulations, each frame of the trajectory was aligned onto a given reference frame (starting structure) by performing a least-squares rotational and translational fit to the P-gp protein backbone. A cubic grid with a spacing of 0.1 nm was then superimposed onto the reference system. The spatial density function for the substrates was then generated by counting the number of times the COM of a given substrate was found within a specific element of the grid using the g_spatial program.[84] The resulting grid was visualized in VMD as an isosurface showing 65% probability of finding either morphine or nicardipine.

Root-Mean-Squared Deviation. As a measure of the difference between configurations extracted from the trajectories or clusters, the RMSD was calculated using the method of Maiorov and Crippin[85] after first performing a rotational and translational fit of each frame of the trajectory to a reference structure or domain.

Cluster Analysis. To determine the relative populations of the conformations of nicardipine, the trajectories were clustered using the method of Daura et al.[86,87] In this work, two conformations were considered to fall within the same cluster if the backbone RMSD between the conformations was <0.15 nm.

Protein and Substrate Contacts. All the protein residues for which the average distance between the centers of at least one atom lay within a 0.3 nm radius of the center of any atom of the given substrate were considered to be in direct contact with the substrate. In all cases the averaging was performed over the last 10 ns of the relevant simulation.

Inter-residue Distances. To compare the distances between specific pairs of amino acids, or between morphine and Gln942, the distance between the center of the representative atoms specified for each group was calculated. Note that the distances used were averaged over the last 10 ns of the relevant simulation.

RESULTS AND DISCUSSION

The PMFs of the two P-gp substrates, morphine and nicardipine were calculated at discrete positions in P-gp along the reaction coordinate (Z) shown in Figure 1. This reaction coordinate passes between the NBDs and the cytosolic parts of P-gp and into the TM pore. Note that a PMF gives the relative free energy with respect to a given reference location along a chosen reaction coordinate (pathway). While the difference in free energy between any two states is independent of the pathway chosen, the shape of the PMF is dependent on the reaction coordinate. In principle, a wide range of alternative reaction coordinates could have been chosen.[88] In this work it is assumed the substrate enters P-gp from the cytoplasm. It has also been proposed that substrate uptake may involve two steps, with substrates first partitioning into the lipid bilayer before binding to P-gp[2]. On the basis of the available crystal structures, two putative substrate uptake portals have been proposed. However, as there is little direct experimental data to support any one proposed pathway over another, the simplest

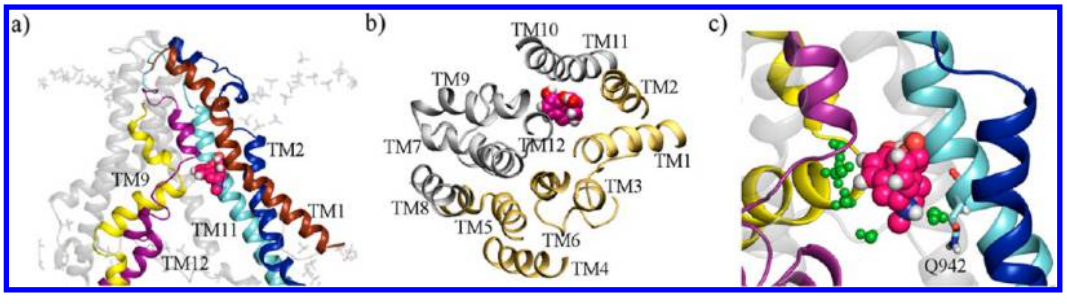

Figure 4. Representative snapshot showing the interaction of morphine with P-gp at its minimum energy well. (a) Front and (b) top views of P-gp (cartoon) showing the position of morphine relative to TM helices 1 (brown), 2 (blue), 9 (yellow), 11 (cyan), and 12 (magenta). (c) A close-up view of bound morphine (pink spacefill) showing water molecules (green spacefill) that hydrogen bond with morphine. Gln942, which has a water-mediated interaction with morphine, is shown in a stick representation. Note: for clarity, TM helices 4 and 5 are not shown in (a) and (c).

DOI: 10.1021/ci5007382
J. Chem. Inf. Model. 2015, 55, 1202−1217

possible reaction coordinate was used in this study. Note that the reference location for the PMF has been chosen as the substrate in aqueous solution (Z = −15 nm). Thus, the difference in free energy between this reference location and the minimum along the reaction coordinate provides an estimate of the free energy of binding to the protein. Figure 3 shows the PMF along the central axis of P-gp for morphine and nicardipine overlaid onto the structure of P-gp.

Potential of Mean Force of Morphine. The PMF of morphine (pink line in Figure 3) progressively decreases as the substrate is moved along the region spanning the NBDs and cytosolic extensions of the TMDs, between Z = −11.0 nm and Z = −4.0 nm. The PMF culminates in a single energy well within the membrane-embedded span of the TM pore (between Z = −4.0 nm and Z = −2.0 nm) located at Z = −2.5 nm. This energy well has a depth of −56 ± 4 kJ/mol relative to the free energy of morphine in bulk solution.

Interaction of Morphine with P-gp. As shown in Figure 1, morphine has a rigid pentacyclic structure and thus, has limited conformational flexibility. The orientation of morphine is not sterically constrained by the protein, and in principle, it could rotate within the TM pore. However, during the simulations morphine primarily adopted a single orientation with respect to the TM helices once it had entered the TM pore, in which the protonated piperidine ring (Figure 1b, ring c) faced toward the water interface. When placed in the energy well shown in Figure 3, morphine binds between TM helices 1, 2, 9, 11, and 12, close to the center of the lipid bilayer as shown in Figure 4a,b. In this conformation, morphine forms direct contacts with 10 residues: Leu64, Met68 (TM1), Tyr113, (TM2), Asn838, Leu839 (TM9), Met945, Tyr946, Ser948, Tyr949 (TM11), and Val978 (TM12). Note that a residue was consider to be in direct contact with the substrate if the average distance, over the last 10 ns of the relevant trajectory, between the center of at least one atom lay within a 0.3 nm radius of the center of any atom of the substrate. A more detailed figure showing the positions of these residues relative to morphine is provided as Figure 5. These residues form stable interactions with morphine that persist throughout the simulation. The protonated piperidine ring (ring c) of morphine forms a hydrogen bond with an adjacent water molecule, which in turn forms a hydrogen bond with the carbonyl group of Gln942 from TM11, as shown in Figure 4c. While the specific water molecule involved varies, this hydrogen bonding pattern persists throughout the simulation. Further details of the water occupancy and distance distribution between the morphine piperidine ring and the side-chain carbonyl of Gln942 is given as Supporting Information (Figure S1).

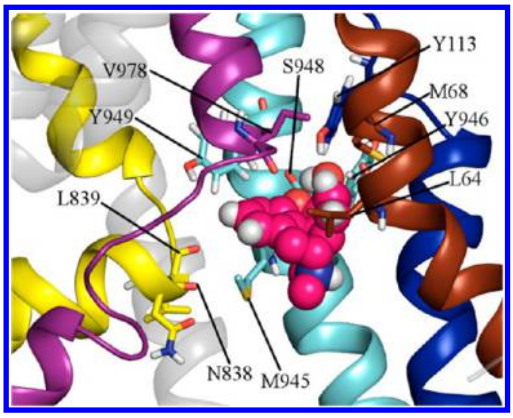

Figure 5. Interaction of morphine with 3G5U P-gp at Z = −2.5 nm. Close-up showing residues that form direct contacts with morphine (spacefill) in the energy well located within the transmembrane pore. The protein backbone is shown in cartoon representation and individual residues are shown in liquorice representation. TM helices 1, 2, 9, 11, and 12 are colored brown, blue, yellow, cyan, and magenta, respectively.

Several of the residues identified have previously been proposed from experimental studies to be involved in the binding or transport of different substrates. For example, Gln942 in TM11 has been proposed to be involved in the binding of verapamil,[24] while verapamil itself has been proposed to bind in a similar location to vinblastine. Photolabeled drug accumulation studies using morphine and verapamil have demonstrated that verapamil competes for binding and transport with morphine.[62] Studies have also shown that the mutation of residues Leu64 and Tyr949 alters the binding affinity of verapamil.[23,26,27] These two residues are among those that form direct contacts with morphine when it resides at the energy minimum identified from the PMF. In the simulations, Leu64 interacted directly with morphine (ring b) and Tyr949 coordinates the allylic hydroxyl of morphine (ring d). Furthermore, these simulations highlighted the role of Tyr113 in the coordination of the phenolic hydroxyl of the morphine (ring a). Several hydrophobic residues have also been shown to influence the binding and transport of vinblastine and verapamil under experimental conditions. Of these, Val978 forms a direct contact with morphine, which persists while morphine is within the energy well (Z = −2.5 nm).

Table 2 lists the residues that interact with morphine at specific locations along the reaction coordinate of the PMF. Several of the residues identified in Figure 5 as interacting with morphine at Z = −2.5 nm have also been proposed to interact with vinblastine. However, the binding of morphine to P-gp also involves residues implicated in the binding of colchicine, which is noncompetitive with the binding of verapamil. This suggests that the site at which morphine interacts with P-gp in MD simulations is not physically distinct from that of colchicine, verapamil, or vinblastine. Again whether a residue was considered to interact with a substrate was based on the distance averaged over 10 ns of the relevant trajectory, not a single snapshot, and thus incorporates local fluctuations.

Potential of Mean Force of Nicardipine. The PMF of nicardipine (blue line in Figure 3) remains relatively flat while nicardipine is moved along the NBDs, between Z = −15 nm and Z = −9 nm. The PMF then gradually decreases along the reaction coordinate, forming two energy wells, one located at in the intracellular lipid−water interface (Z = −4.5 nm) that has a relative depth of −37 ± 4 kJ/mol, and a second, deeper energy well within the TM pore (Z = −2.3 nm) with a relative free energy of −43 ± 5 kJ/mol. The two energy wells are separated by an energy barrier of ∼17 kJ/mol at Z = −3.5 nm. As the energy well in the TM pore has a lower free energy, nicardipine is expected to bind preferentially within the TM pore at a location slightly past the center of the lipid membrane and within the span of the extracellular leaflet.

Interaction of Nicardipine with P-gp. Figure 6 shows representative snapshots from the simulations of nicardipine at the two energy wells corresponding to Z = −4.5 nm and Z = −2.3 nm, as well as the intervening barrier at Z = −3.5 nm. The first energy well at Z = −4.5 nm is located at the intracellular lipid−water interface. Nicardipine is a highly flexible molecule

DOI: 10.1021/ci5007382
J. Chem. Inf. Model. 2015, 55, 1202−1217

Table 2. Residues That Interact with Morphine at Specific Locations along the Reaction Coordinate in the Umbrella Sampling Simulations

amino acid	TM helix no.	reaction coordinate	experimental binding/transport interactions
Gln343	6	Z = −4.5 nm[a]	–
Pro346	6		–
Gln349	6		–
Phe351	6		–
Asn353	6		–
Gln128	3	Z = −3.5 nm[b]	verapamil,[29] vinblastine[29]
Gly868	9		verapamil,[28] vinblastine[17]
Thr941	11		verapamil,[24] vinblastine[24]
Ala943	11		verapamil[24]
Phe979	12		Rhodamine[28]
Ala983	12		colchicine,[28] Rhodamine[28]
Leu64	1	Z = −2.5 nm[c]	verapamil,[27] vinblastine[30]
Met68	1		–
Tyr113	2		–
Asn838	9		–
Leu839	9		–
Gln942	11		verapamil,[24] colchicine[24]
Met945	11		–
Tyr946	11		vinblastine[24]
Ser948	11		–
Tyr949	11		vinblastine,[24] Rhodamine[32]
Val978	12		verapamil,[23,28] vinblastine,[23] colchicine,[23] Rhodamine[31]

[a]Intracellular lipid−water interface. [b]Intermediate region between the lipid−water interface and the energy well of morphine. [c]Energy well within the TM pore, as shown in Figure 3.

and can adopt a variety of alternative conformations, which potentially allow it to form a large number of alternative interactions with P-gp in the simulations. To identify the preferred conformation adopted by nicardipine in this energy well, cluster analysis was performed. Once equilibrated at this location, nicardipine spent the majority of the time in a single conformation (60%, cutoff 0.15 nm) with the top three most populated clusters accounting for 94% of the conformations sampled. Figure 6a shows the central conformation of nicardipine from the dominant cluster. Here, nicardipine adopted an elongated spiral conformation, interacting predominantly with the TM helices 4, 5, and 6 (Figure 6a,b). Two residues, Lys230 and Asp237 (TM4), interacted with the protonated amino benzyl group (Figure 1c, ring a) and the nitrophenyl ring (ring b) of nicardipine, respectively. At this low affinity site, nicardipine also formed direct contacts with residues Ala229, Ser233, Thr236 (TM4), Met295, Gly296, Ala297 (TM5), Gln343, Ser345, and Pro346 (TM6). A snapshot showing these contacts in detail is shown in Figure 7a. These residues line the entrance to the TM pore from the inner lipid leaflet. To date, all inward-facing crystallographic conformations of P-gp and its homologues show a large separation between the cytosolic extensions of TM helices 4 and 6, and also between TM helices 10 and 12, on the opposite side of the TMDs.[4−11] The separation of the helices extends into the membrane-embedded regions of the TMDs, forming two lipid-accessible clefts, proposed by Aller et al. to be substrate uptake portals for hydrophobic P-gp substrates that partition into the cell membrane.[4] Of the residues identified above, Ala229 and Ser345 were reported to be associated with the protrusion of the tail of a lipid into the TM pore in a previous set of MD simulations.[44] This suggests that hydrophobic molecules such as lipids and nicardipine may be able to enter into the TM pore from the membrane, consistent with the proposed "hydrophobic vacuum cleaner" model.[2]

The two energy wells identified in the PMF of nicardipine are separated by an energy barrier of 17 ± 4 kJ/mol at Z = −3.5 nm. As such, this barrier represents a rate-limiting step for the

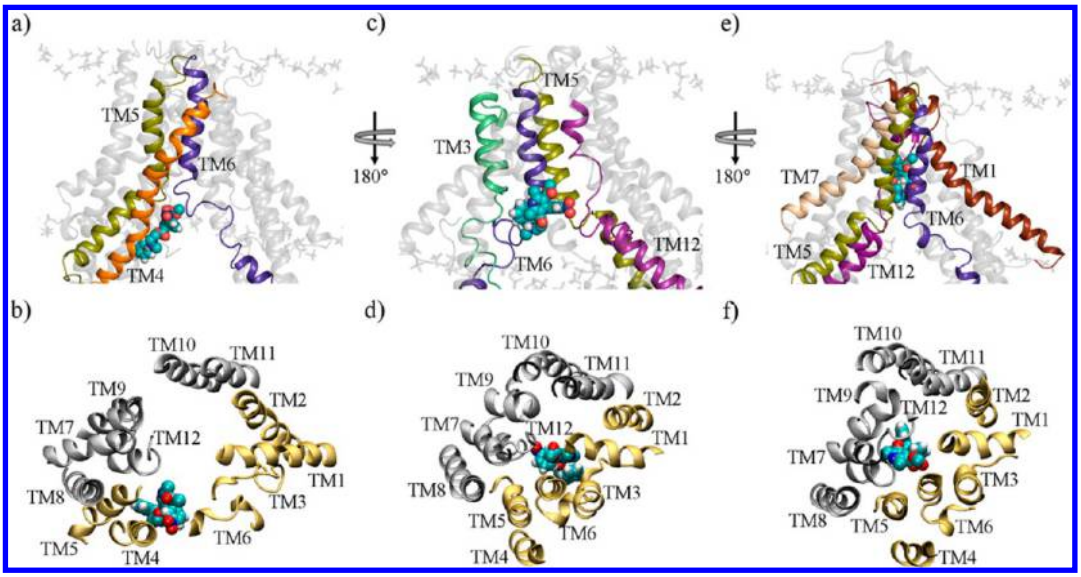

Figure 6. Interaction of nicardipine with P-gp in its two energy wells and at the intervening barrier. (a) Front and (b) top views of the predominant conformation and orientation of nicardipine (cyan spacefill) from cluster analysis, at the first energy well (Z = −4.5 nm) located near the intracellular lipid−water interface, coordinated by TM helices 4 (orange), 5 (olive green), and 6 (purple). (c) Front and (d) top views of nicardipine at the top of the barrier (Z = −3.5 nm), coordinated by TM helices 3 (green), 5 (olive green), 6 (purple), and 12 (magenta). (e) Front and (f) top views of the dominant conformation of nicardipine from cluster analysis, at the second (lowest) energy well (Z = −2.3 nm) located within the TM pore, coordinated by TM helices 1 (brown), 5 (olive green), 6 (purple), 7 (beige), and 12 (magenta).

DOI: 10.1021/ci5007382
J. Chem. Inf. Model. 2015, 55, 1202−1217

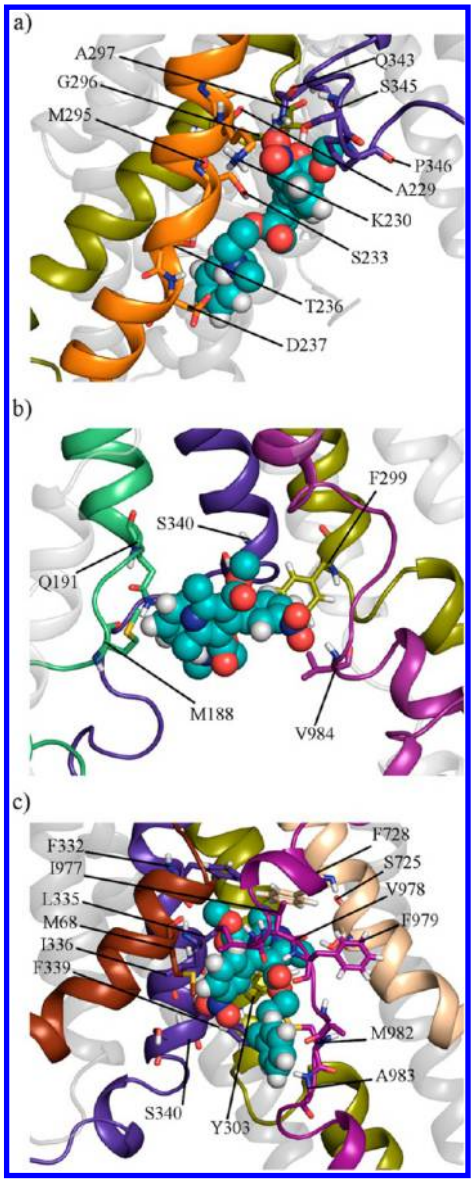

Figure 7. Interaction of nicardipine with 3G5U P-gp at Z = −4.5, −3.5, and −2.3 nm. Close-up showing residues that form direct contacts with nicardipine (spacefill) in (a) the energy well located at the lipid−water interface (Z = −4.5 nm), (b) at the barrier (Z = −3.5 nm), and (c) in the energy well located within the transmembrane pore (Z = −2.3 nm). The protein backbone is shown in cartoon representation and individual residues are shown in liquorice representation. TM 3, 4, 5, 6, 7, and 12 are colored green, orange, olive green, purple, beige, and magenta, respectively.

diffusion of nicardipine to its minimum energy well in the TM pore. Note that this barrier is low enough for nicardipine to cross on a nanosecond time scale and the top of the barrier is still −19 kJ/mol below that of the bulk solution. At the top of the barrier, at Z = −3.5 nm (Figure 6c,d), nicardipine was found to adopt a single conformation in which the molecule was folded so that the amino benzyl group lies parallel to the pyridine ring (ring c) in an apparent $\pi-\pi$ stacking arrangement. In this conformation, nicardipine formed direct contacts with Met188, Gln191 (TM3), Phe299 (TM5), Ser340 (TM6), and Val984 (TM12). Again, a more detailed image is provided as Figure 7b. Of these residues, Val984 has been shown experimentally to affect the transport efficiency of P-gp.[89,90]

The second and deepest energy well of nicardipine (Figure 3) is located within the TM pore at Z = −2.3 nm, just beyond the center of the lipid membrane and within the span of the extracellular leaflet. This well, which is expected to be the primary binding site, has a free energy of −43 ± 5 kJ/mol relative to that of nicardipine in bulk solution. This compares well to the measured binding affinity of P-gp for nicardipine of approximately −30 kJ/mol (K_d = 4.89 ± 0.34 μM).[20] Note that the value from the PMF has not been corrected for concentration effects, as this would require assumptions regarding the volume accessible to the substrate when bound. The corrections for concentration effects are not expected to be large compared to the uncertainty in the calculations and in the experimental data due to differences in the experimental and simulation conditions. Again, cluster analysis was used to identify if nicardipine predominately adopted a single conformation. Five different conformational clusters were identified. Of these the dominant cluster accounted for 67% of total population. In the dominant cluster nicardipine adopted the elongated conformation shown in Figure 6e with the protonated tertiary amine projecting toward the cytosolic water interface, while the pyridine ring (ring c) and the nitrophenyl ring (ring b) of nicardipine were buried deep within the TM pore. The projection of the charged group toward the water is similar to that observed for morphine. As seen in Figure 6f, nicardipine binds between TM helices 1, 5, 6, 7, and 12 and forms direct contacts with residues Met68 (TM1), Tyr303 (TM5), Phe332, Leu335, Ile336, Phe339, Ser340 (TM6), Ser725, Phe728 (TM7), Ile977, Val978, Phe979, Met982, and Ala983 (TM12) (Figure 7c). Note that, although nicardipine predominately adopted an elongated conformation, other conformations were observed, suggesting nicardipine retains a degree of flexibility within the TM pore.

Table 3 lists residues that interact with nicardipine at selected locations along the reaction coordinate of the PMF. Of the 14 residues that interact with nicardipine at Z = −2.3 nm (Figure 7c), corresponding to the deepest energy well, 9 have previously been implicated in the transport and/or binding of verapamil, vinblastine, colchicine, or Rhodamine 123 (Figure 2).[17,22−32] In particular, Leu335 has been shown to play an important role in the transport of all four of these substrates,[22,23,28,30] while Phe332, Leu335, Phe339, Val978, Phe979, Met982, and Ala983 have been specifically implicated in the binding of Rhodamine 123.[28−32] This suggests that nicardipine could bind to P-gp in a similar manner to Rhodamine 123. However, nicardipine was also found to interact with Val978 in the simulations. This residue affects the binding and/or transport of the noncompetitive substrates verapamil and colchicine.[23,26,27] On the basis of the range of interacting residues and the conformational flexibility of nicardipine observed in simulations, it appears that the interaction between nicardipine and P-gp cannot be described in terms of being a distinct binding site.

Substrate Permeation Pathways. Figures 4b and 6f show top views of morphine and nicardipine at their respective lowest energy wells within the TM pore. While morphine and nicardipine both bind within the same general region of P-gp, they interact with residues from different sets of TM helices. In order to understand how the two substrates reach these locations within P-gp, the configurations from the umbrella sampling simulations have been analyzed to construct the lowest energy permeation pathway for each substrate along the chosen reaction coordinate within the confines of the TMD

DOI: 10.1021/ci5007382
J. Chem. Inf. Model. 2015, 55, 1202−1217

Table 3. Residues That Interact with Nicardipine at Specific Locations along the Reaction Coordinate in the Umbrella Sampling Simulations

amino acid	TM helix no.	reaction coordinate	experimental binding/transport interactions
Ala229	4	$Z = -4.5$ nm[a]	–
Lys230	4		–
Ser233	4		–
Thr236	4		–
Asp237	4		–
Met295	5		–
Gly296	5		–
Ala297	5		–
Gln343	6		–
Ser345	6		–
Pro346	6		–
Met188	3	$Z = -3.5$ nm[b]	–
Gln191	3		–
Phe299	5		–
Ser340	6		–
Val984	12		–
Met68	1	$Z = -2.3$ nm[c]	–
Tyr303	5		–
Phe332	6		Rhodamine[28]
Leu335	6		verapamil,[22,28] vinblastine,[23] colchicine,[23] Rhodamine[30]
Ile336	6		–
Phe339	6		Rhodamine[30]
Ser340	6		–
Ser725	7		–
Phe728	7		–
Ile977	12		–
Val978	12		verapamil,[23,28] vinblastine,[23] colchicine,[23] Rhodamine[31]
Phe979	12		Rhodamine[28]
Met982	12		colchicine,[28] Rhodamine[28]
Ala983	12		colchicine,[28] Rhodamine[28]

[a]First energy well at the intracellular lipid–water interface. [b]Energy barrier. [c]Second and deeper energy well within the TM pore, as shown in Figure 3.

pore. Note that this does not exclude other mechanisms by which each substrate may enter the TMD pore.

Figure 8a,b shows the path taken by morphine as it moves from the cytosolic entrance to the TM pore ($Z = -4.5$ nm, blue surface) to its energy well within the TM pore ($Z = -2.5$ nm, red surface). At the cytosolic entrance of the TM pore, morphine formed contacts with residues from TM6, as detailed in Table 2. As morphine entered the TM pore, it interacts with residues from TM3 and TM6 near the cytosolic membrane-water interface before diffusing laterally across the protein, at the level of the cytosolic entrance to the TM pore. Morphine then interacts with TM3 and TM12 and maintains these interactions as it moved deeper into the TM pore to reach its minimum energy well. During this process, it also formed contacts with residues from TM helices 9 and 11.

The permeation pathway identified for morphine contains many residues implicated experimentally in the binding and transport of P-gp substrates. As noted above, morphine initially formed direct contacts with residues from TM6, part of the proposed substrate uptake portals.[4] Morphine also interacts

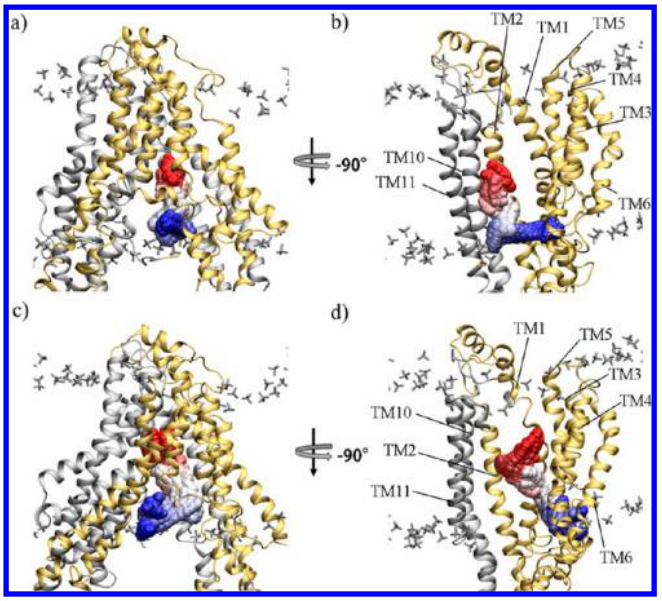

Figure 8. Substrate-specific permeation pathways through the P-gp TM pore. (a) Front and (b) side views of the permeation pathway of morphine from the intracellular lipid–water interface (blue) to its energy well ($Z = -2.5$ nm) within the P-gp TM pore (red). (c) Front and (d) side views of the permeation pathway of nicardipine from the energy well near the intracellular lipid–water interface ($Z = -4.5$ nm, blue), to the energy well within the TM pore ($Z = -2.3$ nm, red). The motion of morphine and nicardipine along their respective pathways are shown using overlapping space filling representations. In (b) and (d) TM helices 7, 8, 9, and 12 are not shown for clarity.

with residues from TM12 that have been proposed to be involved in substrate recognition.[14,15] In addition to these interactions, morphine formed direct contacts with a range of residues along its permeation pathway that are experimentally implicated in the binding or transport of verapamil and/or vinblastine. These include Gln128 (TM3), Gly868 (TM9), Thr941, and Ala943 (TM11) (Table 2). Taken together, this suggests that the pathway identified for morphine may represent a common pathway for other P-gp drug substrates, such as verapamil and vinblastine.

Figure 8c,d shows the permeation pathway of nicardipine as it moves from the cytosolic entrance of the TM pore to its deepest energy well within the TM pore. As nicardipine moves into the cytosolic entrance of the TM pore (corresponding to the first energy well of nicardipine, $Z = -4.5$ nm), it interacts with residues from TM helices 4, 5, and 6 (Figure 8c,d, blue surface). As nicardipine moves deeper into the pore, it crosses an energy barrier of 17 kJ/mol ($Z = -3.5$ nm) and forms contacts with TM helices 6 and 12. After crossing this energy barrier, nicardipine diffuses freely, sampling the entire cross-sectional area of the TM pore. Here nicardipine forms transient contacts with TM helices 1, 3, 5, 6, 7, 9, 11, and 12 (Figure 8c,d, white surface) before reaching the energy well at $Z = -2.3$ nm (Figure 8c,d, red surface) described above. A list of the contact residues for nicardipine along its permeation pathway is also given in Table 3. Notably, Phe190 (TM3) has been implicated in substrate transport.[28] While Phe190 did not make direct contacts with nicardipine in these simulations, nicardipine did make direct contacts with two neighboring residues of Phe190: Met188 and Gln191 (TM3). As stated above, nicardipine also made contacts with a number of other residues previously implicated in the transport and/or binding

DOI: 10.1021/ci5007382
J. Chem. Inf. Model. 2015, 55, 1202–1217

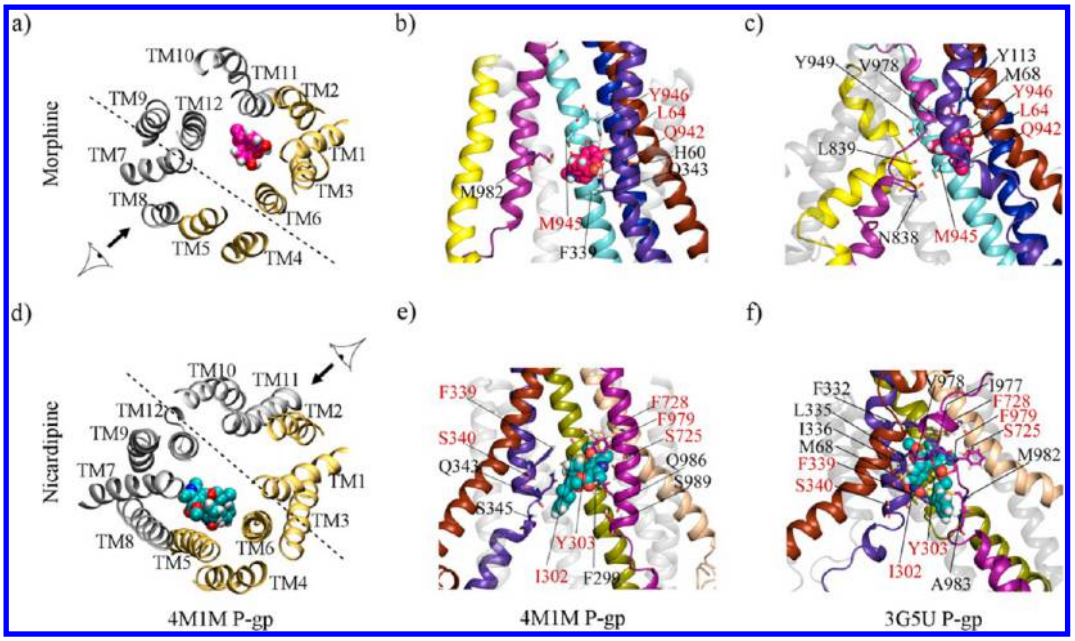

Figure 9. Comparison of the binding sites of morphine (pink spacefill) and nicardipine (cyan spacefill) in membrane-embedded 4M1M and 3G5U P-gp (cartoon representation). (a) Top and (b) front views of morphine bound to equilibrated 4M1M P-gp. Morphine forms close contacts with TM helices 1 (brown), 6 (purple), 11 (cyan), and 12 (magenta). (b) An expanded view of (a) showing residues that interact directly with morphine. (c) Residues interacting with morphine in 3G5U p-gp structure at the minimum energy well (Z = −2.5 nm). (d) Top and (e) front views of nicardipine bound to equilibrated 4M1M P-gp. Nicardipine forms close contacts with TM helices 5 (olive green), 6 (purple), 7 (beige), and 12 (magenta). (e) An expanded view of (d) showing residues that make direct contact with nicardipine. (f) Residues interacting with nicardipine bound to 3G5U P-gp at the lowest energy well (Z = −2.3 nm). The dashed lines in (a) and (d) represent the viewing plane. The arrows represent the direction the plane is viewed in (b) and (c), and in (e) and (f), respectively. The residues labeled in red correspond those observed in both the 4M1M and 3G5U simulations.

of the P-gp substrates verapamil, colchicine, and Rhodamine 123. This suggests that the permeation pathway identified for nicardipine is shared by other classes of P-gp substrates, such as verapamil, colchicine, and Rhodamine 123.

Figure 8 shows that in the simulations morphine and nicardipine take different but overlapping pathways. On the basis of the residues in close contact with morphine and nicardipine, we propose that the morphine permeation pathway is likely to be shared by verapamil and vinblastine, while the nicardipine permeation pathway is likely to be shared by verapamil, colchicine, and Rhodamine 123. Note that, based on the residues identified, the pathway used by verapamil would appear to overlap with both that of morphine and nicardipine. In fact, TM helices 1 and 12 are common to both pathways, indicating that the permeation pathways are not truly distinct. It should be noted that analysis of the permeation pathway has been performed on simulations based on the membrane-embedded, equilibrated 3G5U P-gp structure. Since the current work commenced, a revised structure of mouse P-gp (PDB ID: 4M1M)[11] based on the same diffraction data has been released. There are small differences between TM12 in the original 3G5U and revised 4M1M structures (discussed below), which may result in minor differences between the permeation pathways through each structural model.

Comparison of the Binding of Substrate to Alternate P-gp Structures (3G5U and 4M1M). All of the simulations described above were initially based on the structure of P-gp corresponding to the PDB ID: 3G5U.[4] Although the 3G5U P-gp structure was incorporated into a membrane environment and equilibrated extensively by O'Mara and Mark[51] it is still possible that the simulations presented here have been biased by the choice of starting structure. To investigate this possibility, a series of MD simulations were performed using the revised structure, 4M1M P-gp.[11] The 4M1M P-gp structure was extensively equilibrated in a cholesterol-enriched POPC membrane prior to its use in these simulations. These simulations showed that 4M1M P-gp adopted a conformation consistent to that observed in the equilibrated 3G5U P-gp. Namely, the NBDs moved inward to form a contact interface, while the TMDs maintained a conformation similar to that of the equilibrated 3G5U P-gp. As previously reported in simulations of 3G5U P-gp, some kinking of the TMDs was observed in the vicinity of the endogenous proline residues.[44,51,52] Two simulations were performed in which either a molecule of morphine or a molecule of nicardipine was placed within the TM pore at the position corresponding to the location of their respective free energy minimum obtained from the PMF (Figure 3). The systems were simulated for 40 ns in which morphine or nicardipine was allowed to interact freely with the equilibrated 4M1M P-gp structure. In these simulations, the overall location of morphine and nicardipine in the TM pore was consistent with that obtained using 3G5U P-gp. There were, however, subtle changes in the orientation of both morphine and nicardipine, which lead to some differences in the contact residues within the TM pore between the two P-gp starting conformations.

A comparison of the binding locations and contact residues for morphine and nicardipine in the 4M1M P-gp simulations is shown in Figure 9. Also shown in Figure 9 are the contact residues for morphine and nicardipine in 3G5U P-gp for comparison. From Figure 9a, it can be seen that morphine bound to TM helices 1, 6, 11, and 12 of 4M1M P-gp, forming direct contacts with Leu64 (TM1), Gln942, Met945, and Tyr946 (TM11) (Figure 9b, red). This is consistent with the

DOI: 10.1021/ci5007382
J. Chem. Inf. Model. 2015, 55, 1202−1217

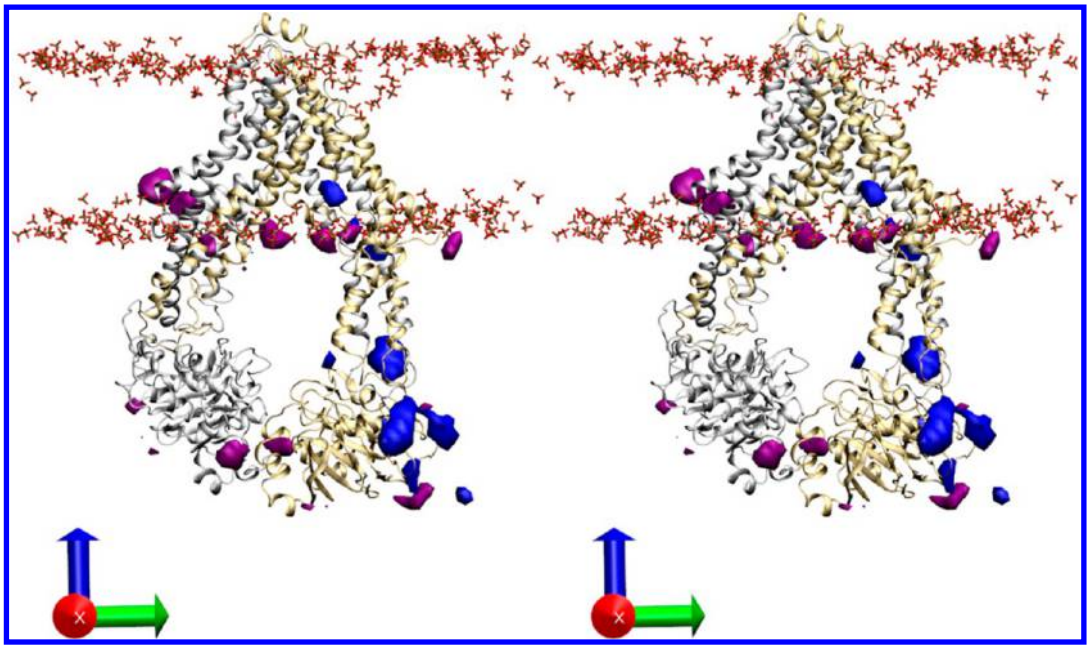

Figure 10. Stereo view of the spatial distribution of morphine and nicardipine around P-gp. Probability isosurfaces for both morphine (pink) and nicardipine (blue) averaged over three independent 80 ns simulations. The surfaces correspond to regions where the probability of finding a given substrate is >65%. The spatial distribution is superimposed over the reference structure of protein shown in cartoon representation.

previous simulations using 3G5U P-gp (Figure 9c, red). In addition, morphine also formed direct contacts with His60 (TM1), Phe339, Glu343 (TM6), and Met982 (TM12) in the 4M1M P-gp simulations. Of these, His60 has been experimentally implicated in the binding of verapamil, vinblastine, and colchicine.[27] It should be noted, however, that Tyr949, which was identified as a contact residue in the 3G5U P-gp simulations (Figure 9c), and is implicated in the binding of verapamil,[24] did not contact morphine in the 4M1M P-gp simulations. Similar changes were noted for nicardipine. Nicardipine formed direct contacts with residues from TM helices 5, 6, 7, and 12 of 4M1M P-gp (Figure 9d). Ile302, Tyr303 (TM5), Phe339, Ser340 (TM6), Ser725, Phe728 (TM7), and Phe979 (TM12) formed direct contacts with nicardipine in both the 4M1M and 3G5U P-gp simulations (indicated in red in Figure 9e,f, respectively). In addition to these residues, nicardipine formed direct contacts with Phe299 (TM5), Gln343, Ser345 (TM6), Gln986, and Ser989 (TM12) in 4M1M P-gp simulations (Figure 9e). As far as we are aware none of these residues have been implicated in the binding or transport of P-gp substrates. In addition to those indicated in red, which were common to both the 4M1M P-gp and the 3G5U P-gp simulations, in the 3G5U P-gp simulation nicardipine also formed direct contacts with Met68, Phe332, Leu335, Ile336, Ile977, Met982, and Ala983. Apart from Met68, each of these residues has been shown to affect the binding or transport of one or more substrates.

When considering the results obtained using 3G5U P-gp and 4M1M P-gp, it is important to note that in their work, O'Mara and Mark found a number of discrepancies between distances inferred from experimental cross-linking distances and the proposed P-gp crystal structure (PDB ID: 3G5U). In particular, O'Mara and Mark demonstrated that after equilibration, the structures sampled in the simulations could better explain cross-linking data involving TM helices 4 and 6 than the proposed 3G5U crystal structure.[51] An expansion of this cross-linking data set, incorporating the 4M1M P-gp crystal structure, is provided as Supporting Information (Table S2). For 50 of the 52 residue pairs, the variation in the distance between paired Cα atoms between the two crystal structures was $\leq$0.3 nm. Of the remaining 2 residue pairs the corresponding distance between the two crystal structures varied by 0.5 nm for the residue pairs 314 (TM5)/749 (TM8), and by 0.6 nm for residues pairs 302 (TM5)/980 (TM12). Discrepancies between the experimental cross-linking data and distances obtained from the crystal structures were noted in the same 20 residue pairs in both 3G5U and 4M1M. This suggests that neither the 3G5U or 4M1M crystal structures satisfy the available cross-linking data better than the other; and neither satisfies the data as well as the ensemble of structures obtained in the simulations starting from either structure. Previous simulation studies have also demonstrated that the TM helices in P-gp are highly flexible.[44,51−53,57] This flexibility was also observed in our simulations of 4M1M P-gp and may be associated with the presence of prolines within the TMDs, in particular, Pro65 (TM1), Pro219 (TM4) Pro346 (TM6), Pro705 (TM7), Pro722 (TM7), Pro862 (TM10), and Pro992 (TM12).[91,92] Overall, the results demonstrate that the work presented here is not heavily influenced by the use of the membrane equilibrated 3G5U P-gp structure as the starting conformation. Specifically, after equilibration in a membrane environment the residues that line the pore and interact with the two substrates are similar using either 3G5U or 4M1M as the starting structure. However, it should be noted that the P-gp TMDs are flexible and that on the time scales used in this work not all of the functionally important contacts may have been sampled.

Spontaneous Binding of Morphine and Nicardipine. To examine the spontaneous binding of morphine and nicardipine to P-gp, two series of simulations were performed, in which either eight molecules of morphine or of nicardipine were placed randomly in solution surrounding the membrane-embedded P-gp and simulated for three times for 80 ns. Both morphine and nicardipine were observed to interact spontaneously with different regions of P-gp. Figure 10 shows a stereo

DOI: 10.1021/ci5007382
J. Chem. Inf. Model. 2015, 55, 1202−1217

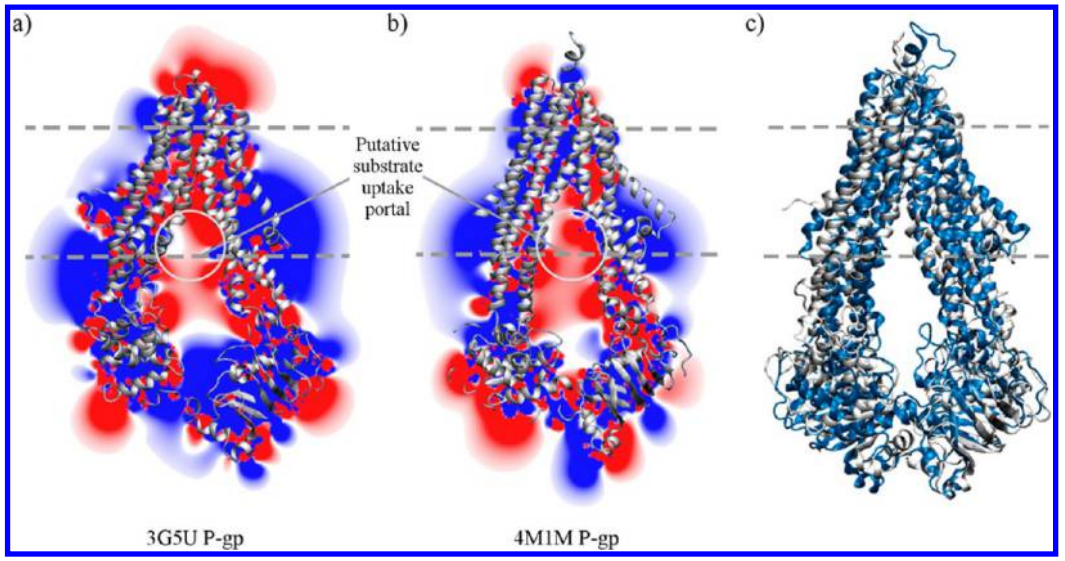

Figure 11. Cross-section of the electrostatic potential of P-gp. A cross-section through the electrostatic potential surface of the MD equilibrated conformations of (a) 3G5U and (b) 4M1M P-gp, taken through the TM pore parallel to the *XZ* plane. The electrostatic potential, contoured at +1 and −1 kT/e, was calculated at pH 7.0 using 150 mM NaCl and a relative dielectric permittivity of 78.5. Negative potential is red, positive is blue. The protein is shown in silver. (c) An overlay of the equilibrated, membrane-embedded structure of 3G5U (silver) and 4M1M (blue) P-gp used in (a) and (b). The dotted lines show the span of the lipid bilayer.

view of the spatial distribution of morphine and nicardipine around P-gp obtained from the simulations. The spatial distribution for the substrates was calculated by averaging the probability of finding either morphine or nicardipine at a specific location after combining the three independent 80 ns simulations. The wire frame surfaces in Figure 10 are contoured at a probability of 65% of finding the substrate at that location during the simulation. The spatial distribution is superimposed onto the starting structure, the equilibrated membrane-embedded 3G5U P-gp. The pink surface and blue surface in Figure 10 correspond to the spatial distribution of morphine and nicardipine, respectively, during the 80 ns of the simulation.

In the case of morphine 12 out of the 24 molecules (50%) bound to the lower lipid leaflet of the membrane. Once bound, these molecules remained in contact with the membrane for the remainder of the time simulated. Six morphine molecules (25%) interacted with the TMDs close to the membrane interface, primarily with TM helices 6 and 7. The final six morphine molecules interacted with negatively charged residues within the NBDs.

In contrast, nicardipine interacted primarily with NBD1 and the cytosolic regions of the TMDs (Figure 10). Specifically, 11 of the 24 molecules (45%) interacted with the cytosolic side of the NBD1, 6 molecules (25%) interacted with the intracellular extension of TM11 and 4 molecules (17%) close to the lipid−water interface in the vicinity of TM helices 2, 3, and 10. The remaining 3 nicardipine molecules formed transient (apparently nonspecific) interactions with NBD2 and other cytosolic regions of TMDs.

The locations identified in Figure 10 at which morphine and nicardipine preferentially interacted with P-gp are associated with regions of negative charge. Approximately 20% of all residues in P-gp are charged at pH 7. The distribution of these residues in 3G5U and 4M1M is given as Supporting Information (Figure S2). The distribution of the positively and negatively charged residues within the protein results in the generation of an electric field surrounding P-gp, which could in principle guide substrates toward the TM pore. Figure 11a,b shows a cross-section of the electrostatic potential surface through the TM pore of 3G5U and 4M1M P-gp, parallel to the *XZ* plane. The electrostatic potential is contoured at +1 and −1 kT/e, assuming a dielectric of 78.5 and 150 mM NaCl. While it should be noted that the exact features of the electrostatic potential are influenced by the precise conformation of the protein at any point in time, it can be seen from Figure 11c that both 3G5U and 4M1M adopt a very similar conformation, and that the cross-section of the electrostatic potential of both 3G5U and 4M1M P-gp contain similar features. There are clear and corresponding regions of net negative potential (red) through the TM pore, in the area surrounding the proposed TM4 and TM6 substrate uptake portal, between the cytosolic extensions of the TMDs and also localized regions of net negative potential in the NBDs. This would be expected to electrostatically steer P-gp substrates, of which almost all are positively charged, toward the TM pore.

■ CONCLUSION

Despite over 30 years of research, the basic question of how drugs bind to and interact with P-glycoprotein is still debated. Experimental approaches have isolated a number of residues that affect substrate binding and transport, but this has not lead to the detailed characterization of the specific substrate binding sites. Theoretical approaches such as rigid-body pharmacophore docking studies have also yielded inconsistent results. To understand the mechanism of drug uptake and binding in a dynamic protein like P-gp more sophisticated approaches are required. Here molecular dynamics simulations have been used to examine the spontaneous binding of the substrates morphine and nicardipine to P-gp, and to calculate their PMF as they move from the aqueous solution along the central axis of P-gp and into the TM pore. These simulations showed that the minimum energy well for both morphine and nicardipine was located within the TM pore, at different but overlapping locations. When residing in their minimum energy locations, both substrates formed direct contacts with residues implicated experimentally in drug binding or transport. However, both

DOI: 10.1021/ci5007382
J. Chem. Inf. Model. 2015, 55, 1202−1217

morphine and nicardipine adopted a range of different orientations (or conformations) within their respective minimum energy wells. As a consequence, it is not possible to allocate specific binding sites to either substrate. Equilibrated, membrane-embedded simulations of the revised 4M1M P-gp structure demonstrate that a core set of residues interacted with either morphine or nicardipine in their minimum energy wells, indicating that the results obtained are not heavily influenced by the choice of starting structure.

The substrate permeation pathway through the TM pore identified from these simulations shows that morphine and nicardipine follow different but overlapping uptake pathways, with TM helices 1 and 12 common to both pathways. Analysis of the residues forming direct contacts with morphine and nicardipine along their respective permeation pathways suggests that the uptake pathways for the canonical P-gp substrates verapamil, vinblastine, colchicine, and Rhodamine 123 may overlap considerably with those identified for morphine and nicardipine. This work demonstrates that neither the drug binding sites nor permeation pathways for morphine and nicardipine are clearly defined in P-gp. This has important consequences for our understanding of P-gp as a multidrug efflux pump, and of the therapeutic strategies used to design selective inhibitors of drug efflux by P-gp. For example, this work suggests that the development of inhibitors that only block the transport of specific substrates may not be possible.

■ ASSOCIATED CONTENT

Supporting Information

Detailed tables showing the equilibration times for each window (Table S1) and a comparison of the 3G5U and 4M1M crystal structures to the cross-linking data (Table S2); and figures showing the interaction between morphine, water and Gln942 (Figure S1), and the distribution of charged residues in P-gp (Figure S2). The Supporting Information is available free of charge on the ACS Publications website at DOI: 10.1021/ci5007382.

■ AUTHOR INFORMATION

Corresponding Author

*E-mail: megan.o'mara@anu.edu.au

Present Address

⊥Research School of Chemistry, Australian National University, Canberra, ACT 0200, Australia

Author Contributions

M.L.O., A.E.M., and N.S. conceived and designed the experiments; N.S. and K.C.J. performed the experiments; N.S. analyzed the data; M.L.O. and A.E.M. contributed reagents/materials/analysis tools; and N.S., A.E.M., and M.L.O. wrote the paper.

Funding

This work was supported by grants from the Australian Research Council (DE120101550, DP110100327), the National Health and Medical Research Council (APP1049685), and the Merit Allocation Scheme on the NCI National Facility at the ANU.

Notes

The authors declare no competing financial interest.

■ ACKNOWLEDGMENTS

M.L.O. is an ARC Discovery Early Career Researcher. A.E.M. is an ARC Discovery Outstanding Researcher.

■ ABBREVIATIONS

P-gp, P-glycoprotein; ABC, ATP-binding cassette; TMD, transmembrane domain; TM, transmembrane; NBD, nucleotide-binding domain; MD, molecular dynamics; ATB, Automated Topology Builder; PMF, potential of mean force

■ REFERENCES

(1) Matheny, C. J.; Lamb, M. W.; Brouwer, K. R.; Pollack, G. M. Pharmacokinetic and Pharmacodynamic Implications of P-glycoprotein Modulation. *Pharmacotherapy* **2001**, *21*, 778−796.

(2) Higgins, C. F.; Gottesman, M. M. Is the Multidrug Transporter a Flippase? *Trends Biochem. Sci.* **1992**, *17*, 18−21.

(3) Dawson, R. J.; Locher, K. P. Structure of a Bacterial Multidrug ABC Transporter. *Nature* **2006**, *443*, 180−185.

(4) Aller, S. G.; Yu, J.; Ward, A.; Weng, Y.; Chittaboina, S.; Zhuo, R.; Harrell, P. M.; Trinh, Y. T.; Zhang, Q.; Urbatsch, I. L.; Chang, G. Structure of P-glycoprotein Reveals a Molecular Basis for Poly-Specific Drug Binding. *Science* **2009**, *323*, 1718−1722.

(5) Hohl, M.; Briand, C.; Grutter, M. G.; Seeger, M. A. Crystal Structure of a Heterodimeric ABC Transporter in its Inward-Facing Conformation. *Nat. Struct Mol. Biol.* **2012**, *19*, 395−402.

(6) Jin, M. S.; Oldham, M. L.; Zhang, Q.; Chen, J. Crystal Structure of the Multidrug Transporter P-glycoprotein from Caenorhabditis Elegans. *Nature* **2012**, *490*, 566−569.

(7) Shintre, C. A.; Pike, A. C.; Li, Q.; Kim, J. I.; Barr, A. J.; Goubin, S.; Shrestha, L.; Yang, J.; Berridge, G.; Ross, J.; Stansfeld, P. J.; Sansom, M. S.; Edwards, A. M.; Bountra, C.; Marsden, B. D.; von Delft, F.; Bullock, A. N.; Gileadi, O.; Burgess-Brown, N. A.; Carpenter, E. P. Structures of ABCB10, a Human ATP-Binding Cassette Transporter in Apo- and Nucleotide-Bound States. *Proc. Natl. Acad. Sci. U.S.A.* **2013**, *110*, 9710−9715.

(8) Kodan, A.; Yamaguchi, T.; Nakatsu, T.; Sakiyama, K.; Hipolito, C. J.; Fujioka, A.; Hirokane, R.; Ikeguchi, K.; Watanabe, B.; Hiratake, J.; Kimura, Y.; Suga, H.; Ueda, K.; Kato, H. Structural Basis for Gating Mechanisms of a Eukaryotic P-glycoprotein Homolog. *Proc. Natl. Acad. Sci. U.S.A.* **2014**, *111*, 4049−4054.

(9) Lee, J. Y.; Yang, J. G.; Zhitnitsky, D.; Lewinson, O.; Rees, D. C. Structural Basis for Heavy Metal Detoxification by an Atm1-Type ABC Exporter. *Science* **2014**, *343*, 1133−1136.

(10) Ward, A. B.; Szewczyk, P.; Grimard, V.; Lee, C. W.; Martinez, L.; Doshi, R.; Caya, A.; Villaluz, M.; Pardon, E.; Cregger, C.; Swartz, D. J.; Falson, P. G.; Urbatsch, I. L.; Govaerts, C.; Steyaert, J.; Chang, G. Structures of P-glycoprotein Reveal Its Conformational Flexibility and an Epitope on the Nucleotide-Binding Domain. *Proc. Natl. Acad. Sci. U.S.A.* **2013**, *110*, 13386−13391.

(11) Li, J.; Jaimes, K. F.; Aller, S. G. Refined Structures of Mouse P-glycoprotein. *Protein Sci.* **2014**, *23*, 34−46.

(12) Martin, C.; Berridge, G.; Mistry, P.; Higgins, C.; Charlton, P.; Callaghan, R. Drug Binding Sites on P-glycoprotein are Altered by ATP Binding Prior to Nucleotide Hydrolysis. *Biochemistry* **2000**, *39*, 11901−11906.

(13) Safa, A. R. Identification and Characterization of the Binding Sites of P-glycoprotein for Multidrug Resistance-Related Drugs and Modulators. *Curr. Med. Chem. Anticancer Agents* **2004**, *4*, 1−17.

(14) Loo, T. W.; Clarke, D. M. Mutational Analysis of ABC Proteins. *Arch. Biochem. Biophys.* **2008**, *476*, 51−64.

(15) Ambudkar, S. V.; Dey, S.; Hrycyna, C. A.; Ramachandra, M.; Pastan, I.; Gottesman, M. M. Biochemical, Cellular, and Pharmacological Aspects of the Multidrug Transporter. *Annu. Rev. Pharmacol. Toxicol.* **1999**, *39*, 361−398.

(16) Qu, Q.; Sharom, F. J. Proximity of Bound Hoechst33342 to the ATPase Catalytic Sites Places the Drug Binding Site of P-glycoprotein within the Cytoplasmic Membrane Leaflet. *Biochemistry* **2002**, *41*, 4744−4752.

(17) Loo, T. W.; Clarke, D. M. Identification of Residues within the Drug-Binding Domain of the Human Multidrug Resistance P-glycoprotein by Cysteine-Scanning Mutagenesis and Reaction with Dibromobimane. *J. Biol. Chem.* **2000**, *275*, 39272−39278.

DOI: 10.1021/ci5007382
J. Chem. Inf. Model. 2015, 55, 1202−1217

(18) Yusa, K.; Tsuruo, T. Reversal Mechanism of Multidrug Resistance by Verapamil: Direct Binding of Verapamil to P-glycoprotein on Specific Sites and Transport of Verapamil Outward across the Plasma Membrane of K562/ADM Cells. *Cancer Res.* **1989**, *49*, 5002−5006.
(19) Tamai, I.; Safa, A. R. Azidopine Noncompetitively Interacts with Vinblastine and Cyclosporin a Binding to P-glycoprotein in Multidrug Resistant Cells. *J. Biol. Chem.* **1991**, *266*, 16796−16800.
(20) Martin, C.; Berridge, G.; Higgins, C. F.; Mistry, P.; Charlton, P.; Callaghan, R. Communication between Multiple Drug Binding Sites on P-glycoprotein. *Mol. Pharmacol.* **2000**, *58*, 624−632.
(21) Pleban, K.; Kopp, S.; Csaszar, E.; Peer, M.; Hrebicek, T.; Rizzi, A.; Ecker, G. F.; Chiba, P. P-glycoprotein Substrate Binding Domains are Located at the Transmembrane Domain/Transmembrane Domain Interfaces: A Combined Photoaffinity Labeling-Protein Homology Modeling Approach. *Mol. Pharmacol.* **2005**, *67*, 365−374.
(22) Loo, T. W.; Clarke, D. M. Defining the Drug-Binding Site in the Human Multidrug Resistance P-glycoprotein Using a Methanethiosulfonate Analog of Verapamil, MTS-Verapamil. *J. Biol. Chem.* **2001**, *276*, 14972−14979.
(23) Loo, T. W.; Clarke, D. M. Identification of Residues in the Drug-Binding Site of Human P-glycoprotein Using a Thiol-Reactive Substrate. *J. Biol. Chem.* **1997**, *272*, 31945−31948.
(24) Loo, T. W.; Clarke, D. M. Identification of Residues in the Drug-Binding Domain of Human P-glycoprotein. Analysis of Transmembrane Segment 11 by Cysteine-Scanning Mutagenesis and Inhibition by Dibromobimane. *J. Biol. Chem.* **1999**, *274*, 35388−35392.
(25) Loo, T. W.; Bartlett, M. C.; Clarke, D. M. Permanent Activation of the Human P-glycoprotein by Covalent Modification of a Residue in the Drug-Binding Site. *J. Biol. Chem.* **2003**, *278*, 20449−20452.
(26) Loo, T. W.; Bartlett, M. C.; Clarke, D. M. Transmembrane Segment 7 of Human P-glycoprotein Forms Part of the Drug-Binding Pocket. *Biochem. J.* **2006**, *399*, 351−359.
(27) Loo, T. W.; Bartlett, M. C.; Clarke, D. M. Transmembrane Segment 1 of Human P-glycoprotein Contributes to the Drug-Binding Pocket. *Biochem. J.* **2006**, *396*, 537−545.
(28) Loo, T. W.; Bartlett, M. C.; Clarke, D. M. Identification of Residues in the Drug Translocation Pathway of the Human Multidrug Resistance P-glycoprotein by Arginine Mutagenesis. *J. Biol. Chem.* **2009**, *284*, 24074−24087.
(29) Parveen, Z.; Stockner, T.; Bentele, C.; Pferschy, S.; Kraupp, M.; Freissmuth, M.; Ecker, G. F.; Chiba, P. Molecular Dissection of Dual Pseudosymmetric Solute Translocation Pathways in Human P-glycoprotein. *Mol. Pharmacol.* **2011**, *79*, 443−452.
(30) Loo, T. W.; Bartlett, M. C.; Clarke, D. M. Suppressor Mutations in the Transmembrane Segments of P-glycoprotein Promote Maturation of Processing Mutants and Disrupt a Subset of Drug-Binding Sites. *J. Biol. Chem.* **2007**, *282*, 32043−32052.
(31) Loo, T. W.; Clarke, D. M. Location of the Rhodamine-Binding Site in the Human Multidrug Resistance P-glycoprotein. *J. Biol. Chem.* **2002**, *277*, 44332−44338.
(32) Donmez Cakil, Y.; Khunweeraphong, N.; Parveen, Z.; Schmid, D.; Artaker, M.; Ecker, G. F.; Sitte, H. H.; Pusch, O.; Stockner, T.; Chiba, P. Pore-Exposed Tyrosine Residues of P-glycoprotein are Important Hydrogen-Bonding Partners for Drugs. *Mol. Pharmacol.* **2014**, *85*, 420−428.
(33) Pascaud, C.; Garrigos, M.; Orlowski, S. Multidrug Resistance Transporter P-glycoprotein has Distinct but Interacting Binding Sites for Cytotoxic Drugs and Reversing Agents. *Biochem. J.* **1998**, *333*, 351−358.
(34) Shapiro, A. B.; Fox, K.; Lam, P.; Ling, V. Stimulation of P-glycoprotein-Mediated Drug Transport by Prazosin and Progesterone. Evidence for a Third Drug-Binding Site. *Eur. J. Biochem.* **1999**, *259*, 841−850.
(35) Shapiro, A. B.; Ling, V. Positively Cooperative Sites for Drug Transport by P-glycoprotein with Distinct Drug Specificities. *Eur. J. Biochem.* **1997**, *250*, 130−137.
(36) Ferreira, R. J.; Ferreira, M. J.; dos Santos, D. J. Molecular Docking Characterizes Substrate-Binding Sites and Efflux Modulation Mechanisms within P-glycoprotein. *J. Chem. Inf. Model.* **2013**, *53*, 1747−1760.
(37) Tarcsay, A.; Keseru, G. M. Homology Modeling and Binding Site Assessment of the Human P-glycoprotein. *Future Med. Chem.* **2011**, *3*, 297−307.
(38) Silva, R.; Carmo, H.; Vilas-Boas, V.; Barbosa, D. J.; Palmeira, A.; Sousa, E.; Carvalho, F.; Bastos Mde, L.; Remiao, F. Colchicine Effect on P-glycoprotein Expression and Activity: In Silico and in Vitro Studies. *Chem. Biol. Interact* **2014**, *218*, 50−62.
(39) Klepsch, F.; Vasanthanathan, P.; Ecker, G. F. Ligand and Structure-Based Classification Models for Prediction of P-glycoprotein Inhibitors. *J. Chem. Inf. Model.* **2014**, *54*, 218−229.
(40) Chufan, E. E.; Kapoor, K.; Sim, H. M.; Singh, S.; Talele, T. T.; Durell, S. R.; Ambudkar, S. V. Multiple Transport-Active Binding Sites are Available for a Single Substrate on Human P-glycoprotein (ABCB1). *PLoS One* **2013**, *8*, No. e82463.
(41) Jara, G. E.; Vera, D. M.; Pierini, A. B. Binding of Modulators to Mouse and Human Multidrug Resistance P-glycoprotein. A Computational Study. *J. Mol. Graph. Model.* **2013**, *46*, 10−21.
(42) Zhang, J.; Sun, T.; Liang, L.; Wu, T.; Wang, Q. Drug Promiscuity of P-glycoprotein and Its Mechanism of Interaction with Paclitaxel and Doxorubicin. *Soft Matter* **2014**, *10*, 438−445.
(43) Ma, J.; Biggin, P. C. Substrate Versus Inhibitor Dynamics of P-glycoprotein. *Proteins* **2013**, *81*, 1653−1668.
(44) Wen, P. C.; Verhalen, B.; Wilkens, S.; McHaourab, H. S.; Tajkhorshid, E. On the Origin of Large Flexibility of P-glycoprotein in the Inward-Facing State. *J. Biol. Chem.* **2013**, *288*, 19211−19220.
(45) Jones, P. M.; George, A. M. Mechanism of ABC Transporters: A Molecular Dynamics Simulation of a Well Characterized Nucleotide-Binding Subunit. *Proc. Natl. Acad. Sci. U.S.A.* **2002**, *99*, 12639−12644.
(46) Jones, P. M.; George, A. M. Nucleotide-Dependent Allostery within the ABC Transporter ATP-Binding Cassette: A Computational Study of the MJ0796 Dimer. *J. Biol. Chem.* **2007**, *282*, 22793−22803.
(47) Campbell, J. D.; Sansom, M. S. Nucleotide Binding to the Homodimeric MJ0796 Protein: A Computational Study of a Prokaryotic ABC Transporter NBD Dimer. *FEBS Lett.* **2005**, *579*, 4193−4199.
(48) Wen, P. C.; Tajkhorshid, E. Dimer Opening of the Nucleotide Binding Domains of ABC Transporters after ATP Hydrolysis. *Biophys. J.* **2008**, *95*, 5100−5110.
(49) Jones, P. M.; George, A. M. Opening of the ADP-Bound Active Site in the ABC Transporter ATPase Dimer: Evidence for a Constant Contact, Alternating Sites Model for the Catalytic Cycle. *Proteins* **2009**, *75*, 387−396.
(50) Damas, J. M.; Oliveira, A. S.; Baptista, A. M.; Soares, C. M. Structural Consequences of ATP Hydrolysis on the ABC Transporter NBD Dimer: Molecular Dynamics Studies of HlyB. *Protein Sci.* **2011**, *20*, 1220−1230.
(51) O'Mara, M. L.; Mark, A. E. The Effect of Environment on the Structure of a Membrane Protein: P-glycoprotein under Physiological Conditions. *J. Chem. Theory Comput.* **2012**, *8*, 3964−3976.
(52) O'Mara, M. L.; Mark, A. E. Structural Characterization of Two Metastable ATP-Bound States of P-glycoprotein. *PLoS One* **2014**, *9*, No. e91916.
(53) Wise, J. G. Catalytic Transitions in the Human MDR1 P-glycoprotein Drug Binding Sites. *Biochemistry* **2012**, *51*, 5125−5141.
(54) Ferreira, R. J.; Ferreira, M.-J. U.; dos Santos, D. J. V. A. Insights on P-glycoprotein's Efflux Mechanism Obtained by Molecular Dynamics Simulations. *J. Chem. Theory Comput.* **2012**, *8*, 1853−1864.
(55) Oliveira, A. S.; Baptista, A. M.; Soares, C. M. Conformational Changes Induced by ATP-Hydrolysis in an ABC Transporter: A Molecular Dynamics Study of the Sav1866 Exporter. *Proteins* **2011**, *79*, 1977−1990.
(56) Becker, J. P.; Depret, G.; van Bambeke, F.; Tulkens, P. M.; Prevost, M. Molecular Models of Human P-glycoprotein in Two Different Catalytic States. *BMC Struct. Biol.* **2009**, *9*, 3−21.

DOI: 10.1021/ci5007382
J. Chem. Inf. Model. 2015, 55, 1202−1217

(57) Liu, M.; Hou, T.; Feng, Z.; Li, Y. The Flexibility of P-glycoprotein for Its Poly-Specific Drug Binding from Molecular Dynamics Simulations. *J. Biomol. Struct. Dyn.* **2013**, *31*, 612−629.
(58) Watanabe, Y.; Hsu, W.-L.; Chiba, S.; Hayashi, T.; Furuta, T.; Sakurai, M. Dynamics and Structural Changes Induced by ATP and/or Substrate Binding in the Inward-Facing Conformation State of P-glycoprotein. *Chem. Phys. Lett.* **2013**, *557*, 145−149.
(59) Klepsch, F.; Chiba, P.; Ecker, G. F. Exhaustive Sampling of Docking Poses Reveals Binding Hypotheses for Propafenone Type Inhibitors of P-glycoprotein. *PLoS Comput. Biol.* **2011**, *7*, No. e1002036.
(60) Gach, K.; Wyrebska, A.; Fichna, J.; Janecka, A. The Role of Morphine in Regulation of Cancer Cell Growth. *Naunyn Schmiedebergs Arch. Pharmacol.* **2011**, *384*, 221−230.
(61) Rasmussen, M.; Zhu, W.; Tonnesen, J.; Cadet, P.; Tonnesen, E.; Stefano, G. B. Effects of Morphine on Tumour Growth. *Neuroendocrinol. Lett.* **2002**, *23*, 193−198.
(62) Callaghan, R.; Riordan, J. R. Synthetic and Natural Opiates Interact with P-glycoprotein in Multidrug-Resistant Cells. *J. Biol. Chem.* **1993**, *268*, 16059−16064.
(63) Katoh, M.; Nakajima, M.; Yamazaki, H.; Yokoi, T. Inhibitory Potencies of 1,4-Dihydropyridine Calcium Antagonists to P-glycoprotein-Mediated Transport: Comparison with the Effects on CYP3A4. *Pharm. Res.* **2000**, *17*, 1189−1197.
(64) Ibrahim, S.; Peggins, J.; Knapton, A.; Licht, T.; Aszalos, A. Influence of Antipsychotic, Antiemetic, and Ca(2+) Channel Blocker Drugs on the Cellular Accumulation of the Anticancer Drug Daunorubicin: P-glycoprotein Modulation. *J. Pharmacol. Exp. Ther.* **2000**, *295*, 1276−1283.
(65) Malde, A. K.; Zuo, L.; Breeze, M.; Stroet, M.; Poger, D.; Nair, P. C.; Oostenbrink, C.; Mark, A. E. An Automated Force Field Topology Builder (ATB) and Repository: Version 1.0. *J. Chem. Theory Comput.* **2011**, *7*, 4026−4037.
(66) van der Spoel, D.; Lindahl, E.; Hess, B.; Groenhof, G.; Mark, A. E.; Berendsen, H. J. Gromacs: Fast, Flexible, and Free. *J. Comput. Chem.* **2005**, *26*, 1701−1718.
(67) Schmid, N.; Eichenberger, A. P.; Choutko, A.; Riniker, S.; Winger, M.; Mark, A. E.; van Gunsteren, W. F. Definition and Testing of the GROMOS Force-Field Versions 54A7 and 54B7. *Eur. Biophys. J.* **2011**, *40*, 843−856.
(68) Hermans, J.; Berendsen, H. J. C.; van Gunsteren, W. F.; Postma, J. P. M. A Consistent Empirical Potential for Water-Protein Interactions. *Biopolymers* **1984**, *23*, 1513−1518.
(69) Poger, D.; van Gunsteren, W. F.; Mark, A. E. A New Force Field for Simulating Phosphatidylcholine Bilayers. *J. Comput. Chem.* **2010**, *31*, 1117−1125.
(70) Tironi, I. G.; Sperb, R.; Smith, P. E.; van Gunsteren, W. F. A Generalized Reaction Field Method for Molecular-Dynamics Simulations. *J. Chem. Phys.* **1995**, *102*, 5451−5459.
(71) Heinz, T. N.; van Gunsteren, W. F.; Hunenberger, P. H. Comparison of Four Methods to Compute the Dielectric Permittivity of Liquids from Molecular Dynamics Simulations. *J. Chem. Phys.* **2001**, *115*, 1125−1136.
(72) Hess, B.; Bekker, H.; Berendsen, H. J. C.; Fraaije, J. G. E. M. LINCS: A Linear Constraint Solver for Molecular Simulations. *J. Comput. Chem.* **1997**, *18*, 1463−1472.
(73) Miyamoto, S.; Kollman, P. A. SETTLE—An Analytical Version of the Shake and Rattle Algorithm for Rigid Water Models. *J. Comput. Chem.* **1992**, *13*, 952−962.
(74) Feenstra, K. A.; Hess, B.; Berendsen, H. J. C. Improving Efficiency of Large Time-Scale Molecular Dynamics Simulations of Hydrogen-Rich Systems. *J. Comput. Chem.* **1999**, *20*, 786−798.
(75) Berendsen, H. J. C.; Postma, J. P. M.; van Gunsteren, W. F.; Dinola, A.; Haak, J. R. Molecular-Dynamics with Coupling to an External Bath. *J. Chem. Phys.* **1984**, *81*, 3684−3690.
(76) Humphrey, W.; Dalke, A.; Schulten, K. VMD: Visual Molecular Dynamics. *J. Mol. Graphics* **1996**, *14* (33−38), 27−38.
(77) Loo, T. W.; Clarke, D. M. Drug-Stimulated ATPase Activity of Human P-glycoprotein Requires Movement between Transmembrane Segments 6 and 12. *J. Biol. Chem.* **1997**, *272*, 20986−20989.
(78) Szegezdi, J.; Csizmadia, F. Prediction of Dissociation Constant Using Microconstants. Presented at the 227th ACS National Meeting, Anaheim, CA, Mar 28−Apr 1, 2004.
(79) Szegezdi, J.; Csizmadia, F. A Method for Calculating the Pka Values of Small and Large Molecules. Presented at the 233rd ACS National Meeting, Chicago, IL, Mar 25−29, 2007.
(80) Koziara, K. B.; Stroet, M.; Malde, A. K.; Mark, A. E. Testing and Validation of the Automated Topology Builder (ATB) Version 2.0: Prediction of Hydration Free Enthalpies. *J. Comput. Aided Mol. Des* **2014**, *28*, 221−233.
(81) Torrie, G. M.; Valleau, J. P. Nonphysical Sampling Distributions in Monte Carlo Free-Energy Estimation: Umbrella Sampling. *J. Comput. Phys.* **1977**, *23*, 187−199.
(82) Kästner, J.; Thiel, W. Bridging the Gap between Thermodynamic Integration and Umbrella Sampling Provides a Novel Analysis Method: "Umbrella Integration". *J. Chem. Phys.* **2005**, *123*, No. 144104.
(83) Kästner, J.; Thiel, W. Analysis of the Statistical Error in Umbrella Sampling Simulations by Umbrella Integration. *J. Chem. Phys.* **2006**, *124*, No. 234106.
(84) Lindahl, E.; Hess, B.; van der Spoel, D. Gromacs 3.0: A Package for Molecular Simulation and Trajectory Analysis. *J. Mol. Model.* **2001**, *7*, 306−317.
(85) Maiorov, V. N.; Crippen, G. M. Significance of Root-Mean-Square Deviation in Comparing Three-Dimensional Structures of Globular Proteins. *J. Mol. Biol.* **1994**, *235*, 625−634.
(86) Daura, X.; van Gunsteren, W. F.; Mark, A. E. Folding-Unfolding Thermodynamics of a Beta-Heptapeptide from Equilibrium Simulations. *Proteins* **1999**, *34*, 269−280.
(87) Daura, X.; Gademann, K.; Jaun, B.; Seebach, D.; van Gunsteren, W. F.; Mark, A. E. Peptide Folding: When Simulation Meets Experiment. *Angew. Chem., Int. Ed.* **1999**, *38*, 236−240.
(88) de Ruiter, A.; Oostenbrink, C. Protein−Ligand Binding from Distancefield Distances and Hamiltonian Replica Exchange Simulations. *J. Chem. Theory Comput.* **2013**, *9*, 883−892.
(89) Crowley, E.; O'Mara, M. L.; Reynolds, C.; Tieleman, D. P.; Storm, J.; Kerr, I. D.; Callaghan, R. Transmembrane Helix 12 Modulates Progression of the ATP Catalytic Cycle in ABCB1. *Biochemistry* **2009**, *48*, 6249−6258.
(90) Mandal, D.; Moitra, K.; Ghosh, D.; Xia, D.; Dey, S. Evidence for Modulatory Sites at the Lipid-Protein Interface of the Human Multidrug Transporter P-glycoprotein. *Biochemistry* **2012**, *51*, 2852−2866.
(91) Liang, J.; Naveed, H.; Jimenez-Morales, D.; Adamian, L.; Lin, M. Computational Studies of Membrane Proteins: Models and Predictions for Biological Understanding. *Biochim. Biophys. Acta* **2012**, *1818*, 927−941.
(92) Senes, A.; Engel, D. E.; DeGrado, W. F. Folding of Helical Membrane Proteins: The Role of Polar, GxxxG-Like and Proline Motifs. *Curr. Opin Struct. Biol.* **2004**, *14*, 465−479.

DOI: 10.1021/ci5007382
J. Chem. Inf. Model. 2015, 55, 1202−1217